Electron-ion Coulomb scattering and the electron Landau damping of Alfvén waves in the solar wind

Joseph E. Borovsky[1,2] and S. Peter Gary[1]

Received 23 December 2010; revised 9 March 2011; accepted 4 April 2011; published 6 July 2011.

[1] All Alfvén waves in the solar wind have parallel electric fields, which enable Landau damping. The Alfvén waves' Landau resonate with very low energy electrons; low-energy electrons are easily trapped in the Alfvén waves, and at low energies electron-ion Coulomb scattering is very rapid. Analytic fluid theory and numerical solutions to the linear Vlasov equation are used to determine the properties of Alfvén waves (and kinetic Alfvén waves) in the solar wind. Electrostatic potentials associated with the waves' parallel electric fields are found to be relatively large. Owing to the large potentials, electrons over a broad range of velocities interact with the wave to produce Landau damping. Because of this broad range, linear Vlasov theory is invalid and the Landau-damping rates computed via linear Vlasov theory may not be accurate. Electron velocity diffusion owed to electron-ion Coulomb scattering is analyzed. Electron diffusion times in the Alfvén wave Landau resonance are calculated and are found to be faster than wave periods and much faster than Landau-damping time scales. Coulomb collisions should prevent the electron distribution function from evolving away from a Maxwellian form, and thereby Coulomb collisions act to maintain Landau damping (although at a rate different than that given by linear Vlasov theory). Some complications of this Landau-damping picture arise from the interplanetary electric field competing with the Alfvén wave parallel electric fields and from ion beams near the Landau resonance.

Citation: Borovsky, J. E., and S. P. Gary (2011), Electron-ion Coulomb scattering and the electron Landau damping of Alfvén waves in the solar wind, *J. Geophys. Res.*, *116*, A07101, doi:10.1029/2010JA016403.

1. Introduction

[2] Since the solar wind is not an infinite homogeneous plasma [e.g., *Burlaga*, 1968, 1969, 1971; *Bruno et al.*, 2001; *Riazantseva et al.*, 2005; *Borovsky*, 2008, 2010], all Alfvén waves in the solar wind have $k_\perp \neq 0$. Owing to the divergence of the ion polarization drift, all Alfvén waves with $k_\perp \neq 0$ have parallel electric fields [*Fejer and Kan*, 1969; *Goertz and Boswell*, 1979; *Goertz*, 1984; *Thompson and Lysak*, 1996; *Hollweg*, 1999]. This parallel electric field makes all Alfvén waves subject to dissipation by Landau damping [*Stepanov*, 1958; *Fejer and Kan*, 1969; *Stéfant*, 1970; *Gary and Borovsky*, 2008].

[3] For Alfvén waves in the solar wind, Landau damping is important. The $k_\perp$ cascade of MHD turbulence in the solar wind is believed to be dissipated at high $k_\perp$ by Landau damping on solar wind electrons and ions [*Dobrowolny and Torricelli-Ciamponi*, 1985; *Leamon et al.*, 1999; *Gary and Borovsky*, 2004; *Howes et al.*, 2008] (but see *Parashar et al.* [2009] for an alternative), and at all values of $k_\perp$ the dissipation of Alfvénically propagating flow shears by Landau damping provides a coefficient of shear viscosity for the solar wind [*Borovsky and Gary*, 2009]. For $\beta_i < 1$ (which is typical in the solar wind at 1 AU), electron Landau damping dominates over ion Landau damping [*Stéfant*, 1970; *Gary and Borovsky*, 2008; *Borovsky and Gary*, 2009; *Sahraoui et al.*, 2010].

[4] In the absence of collisions, Landau damping of waves will result in a modification of the distribution function at the resonant velocity owing to particle trapping [e.g., *Knorr*, 1963; *Gary*, 1967] (compare section 10.4 of *Krall and Trivelpiece*'s [1973] work and section 4.2.3 of *Davidson*'s [1972] work). This modification occurs on the time scale of the trapped-particle bounce time τ_b. For electron Landau damping of Alfvén waves owing to the nonzero parallel electric field of the wave [*Stepanov*, 1958; *Fejer and Kan*, 1969; *Stéfant*, 1970; *Gary and Borovsky*, 2008], a flattening of the electron velocity distribution function (plateau formation) near $v_\parallel = v_A$ should occur, reducing the strength of Landau damping, which is proportional to $\partial f/\partial v_\parallel$ at $v_\parallel = v_A$. In a truly collisionless plasma this could happen. However, at the $v_\parallel \approx v_A$ resonance in the solar wind, the electron-ion collision times can be very short, a second or less, much shorter than wave periods. This fast collision time can act to ruin plateau formation in the electron velocity distribution

[1]Space Science and Applications, Los Alamos National Laboratory, Los Alamos, New Mexico, USA.
[2]Also at Department of Atmospheric, Oceanic, and Space Sciences, University of Michigan, Ann Arbor, Michigan, USA.

0148-0227/11/2010JA016403

Table 1. Typical Solar Wind Parameters at 1 AU[a]

Symbol	Value	Definition
N	6 cm^{-3}	Number density
T_e	15 eV	electron temperature (core)
T_i	7 eV	Proton temperature
B_o	6×10^{-5} gauss	magnetic field strength
v_{Te}	1630 km/s	Electron thermal speed
v_{Ti}	26 km/s	ion thermal speed
C_s	51 km/s	ion-acoustic speed
v_A	54 km/s	Alfvén speed
$\tau_{ce} = 2\pi/\omega_{ce}$	5.9×10^{-3} s	electron-cyclotron period
$\tau_{ci} = 2\pi/\omega_{ci}$	11 s	proton-cyclotron period
τ_{ei}	1.9×10^4 s	electron-ion 90° collision time
τ_{ii}	1.2×10^5 s	ion-ion 90° collision time
τ_{ee}	8.4×10^3 s	electron-electron 90° collision time
$r_{gi} = v_{Ti}/\omega_{ci}$	45 km	thermal ion gyroradius
$L = C_s/\omega_{ci}$	88 km	ion acoustic gyroradius
c/ω_{pe}	26 km	electron skin depth
c/ω_{pi}	113 km	ion inertial length
λ_{De}	800 cm	Debye length
β_i	0.47	ion beta
β_e	1.0	electron beta
B	1.5	total plasma beta
$\sigma_\parallel$	2.9×10^{13} s^{-1}	parallel electrical conductivity
σ_P	0.072 s^{-1}	Pedersen conductivity

[a]From *Borovsky and Gary* [2008].

function and continuously force the electron distribution function back to a Maxwellian form. This collisional process has been quantified for plateau formation owing to the electron Landau damping of Langmuir waves [*Zakharov and Karpman*, 1963; *Denavit et al.*, 1968; *Johnston*, 1971; *Auerbach*, 1977; *Bilato and Brambilla*, 2008]. Similar arguments about collisions have been made for the electron Landau damping of Alfvén waves [*Potapenko et al.*, 2000] and of nonlinearly steepened Alfvén waves [*Medvedev et al.*, 1998; *Medvedev*, 1999].

[5] Note that it has been argued that the addition of a small amount of scattering will not change the linear Landau-damping coefficient for Langmuir waves: Rather, it adds a second collisional damping coefficient [*Comisar*, 1963; *Burgers*, 1963]. For a small amount of scattering this should similarly be the case for Alfvén waves, with Landau damping being accompanied by a shear viscosity damping [e.g., *Braginskii*, 1965, equation (8.40)] of and a Pedersen conductivity damping [e.g., *Borovsky*, 1993, equation (A4)]. An argument as to why the Landau damping does not change even when electrons are scattered out of resonance is based on the point that, statistically, for every electron scattered out of resonance one is scattered into the resonance: The Maxwellian distribution is maintained by collisions and the phase-space elements that participate in the Landau damping are always populated. Note, however, that for Alfvén waves with periods on the order of the electron-ion collision time τ_{ei} it is expected that the electron-Landau-damping resonance at $v_\parallel \approx v_A$ will be broadened and that the electron Landau damping will be reduced [cf. *Hedrick et al.*, 1995].

[6] Coulomb collisions acting on particles in the Landau resonance provide the pathway for entropy changes in the plasma via the Landau damping of wave energy [*Auerbach*, 1977] and makes Landau damping irreversible [e.g., *Ryutov*, 1999]. Electron-ion Coulomb scattering enables energy and momentum exchange between electrons and ions (compare with section 7–7 of *Shkarofsky et al.*'s [1966] work).

[7] Typical solar wind parameters at 1 AU are listed in Table 1. The characteristic velocities in the solar wind plasma are v_A = 54 km/s, v_{Ti} = 26 km/s, and v_{Te} = 1630 km/s. In Figure 1 the reduced electron and proton distribution functions $f(v_\parallel)$ are plotted in the vicinity of the $v_\parallel \approx v_A$ Landau resonance for these typical solar wind parameters, assuming the distribution functions to be Maxwellians. Note the relative flatness of the electron distribution function in the region of resonance. In Figure 1 the parallel kinetic energies of the electrons are denoted in green. Note that the parallel kinetic energies $E_\parallel$ of the electrons at this Alfvén speed resonance are quite small: $E_\parallel = m_e v_A^2/2 = 8.3 \times 10^{-3}$ eV. With the solar wind electrons composed of a core plus halo population [*Feldman et al.*, 1975; *Skoug et al.*, 2000] with core population temperatures of 12 ± 3 eV and halo population temperatures of 83 ± 22 eV, the electrons at the Alfvén speed resonance are in the "core of the core" of the electrons. Even with the solar wind ram velocity, this region of the solar wind electron distribution function is of too low an energy to be accessible to measurement (Ruth Skoug, private communication, 2010) owing to (1) the low-energy cutoffs of electron instruments, (2) spacecraft charging with respect to infinity, (3) the space-charge potential of spacecraft photoelectron clouds, and (4) the contamination of the electron population by spacecraft-generated photoelectrons [e.g., *Isensee and Maassberg*, 1981; *Scime et al.*, 1994; *Katz et al.*, 2001; *Salem et al.*, 2001].

[8] In this paper the properties of Alfvén waves and kinetic Alfvén waves in the solar wind are examined, and the roles of electron trapping and electron-ion Coulomb scattering are explored. This paper is organized as follows. In section 2, electron-ion Coulomb scattering time scales are calculated. In section 3 the parallel electric fields and the electrostatic potentials of Alfvén waves are explored. In section 4 the role of electron-ion Coulomb scattering on disrupting electron trapping in Alfvén waves is explored. The results of this study are summarized in section 5, where an assessment is made for the state of electron Landau damping in the solar wind. Section 6 contains a discussion of other factors that complicate the picture of Landau damping in the solar wind, and section 7 contains a discussion on the impact of this work on previous results.

2. Electron-Ion Coulomb Scattering Times on the Resonance Plane

[9] In Figure 2 the Alfvén speed resonance plane is shown in red in $v_\parallel - v_\perp$ space relative to the ion thermal speed (inner black sphere) and the electron thermal speed (outer black sphere). Except for the small region of the resonance plane where $v_\perp$ is small, electrons on the resonance plane have pitch angles near 90°. To determine the effect of electron-ion Coulomb collisions on electron Landau damping, it is relevant to calculate the electron-ion Coulomb scattering times for electrons on this resonance plane.

[10] For electron-ion Coulomb collisions, the rule-of-thumb gauge of the collisionality of a population of electrons in a plasma is the 90° random walk time τ_{ei} for electrons at the electron thermal velocity. This 90° scattering time at the thermal speed can be written [e.g., *Neufeld and Ritchie*, 1955, equation (33); *Krall and Trivelpiece*, 1973, equation (6.4.10)]

$$\tau_{ei} = m_e^2 \, v_{Te}^3 / 8 \, \pi \, n \, e^4 \log_e(\Lambda), \quad (1)$$

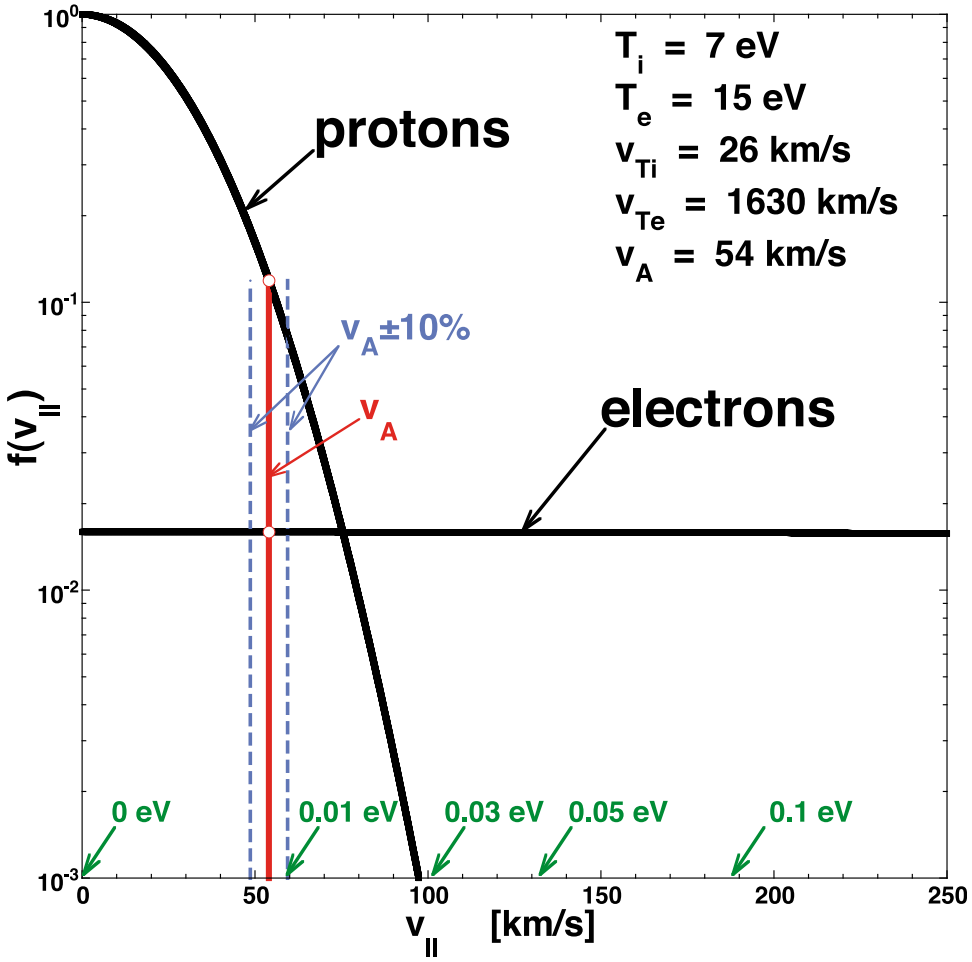

Figure 1. A sketch of the electron and proton velocity distribution functions of the solar wind at 1 AU in the vicinity of the $v_{\parallel} \sim v_A$ Landau resonance. For the sketch, the distribution functions are taken to be Maxwellians. The kinetic energies of electrons are noted in green.

where $\log_e(\Lambda) = \log_e(12\pi N)$ is the Coulomb logarithm, with $N = n\lambda_{De}^3$ being the number of electrons per cubic Debye length in the plasma. The τ_{ei} of expression (1) is the time scale for the velocity vector of a thermal electron to random walk through 90° owing to multiple small-angle scattering. For the typical solar wind parameters of Table 1 (with $\log_e(\Lambda) = 26.6$), expression (1) yields $\tau_{ei} = 1.9 \times 10^4$ s = 5.3 h for the rule-of-thumb 90° electron-ion collision time scale in the solar wind at 1 AU.

[11] But sometimes the time scale for velocity diffusion over smaller scales is relevant, and for electrons at other than the thermal speed. For instance, the time to diffuse electrons out of a Landau resonance is much less than the time to diffuse thermal electrons by 90°. The electrons in a local element of the electron velocity distribution function will undergo multiple Coulomb scattering off the protons and will diffuse in angle according to

$$\partial f/\partial t = D_{\theta\theta}\, \partial^2 f/\partial\theta^2 \tag{2}$$

(compare with *Scott*'s [1963] equation (2.48) and discussion thereafter). Here $D_{\theta\theta}$ is a diffusion coefficient representing the collision frequency of electron-proton Coulomb interactions. The solution to expression (2) is

$$f(\theta, t) = (4\pi D_{\theta\theta} t)^{-1/2} \exp\left(-\theta^2/4D_{\theta\theta} t\right). \tag{3}$$

This is a Gaussian distribution of angle θ with a half-width θ_o given by

$$\theta_o = (D_{\theta\theta} t)^{1/2}. \tag{4}$$

According to expression (4), the time to evolve from a delta function at t = 0 to a Gaussian with half-width θ_o is

$$t = \theta_o^2/4D_{\theta\theta}. \tag{5}$$

According to expression (5), the time $\tau_{\Delta\theta}$ to scatter by a small angle $\Delta\theta$ compared with the time τ_{90} to scatter by 90° is

$$\tau_{\Delta\theta} = \tau_{90}(\Delta\theta/90^\circ)^2. \tag{6}$$

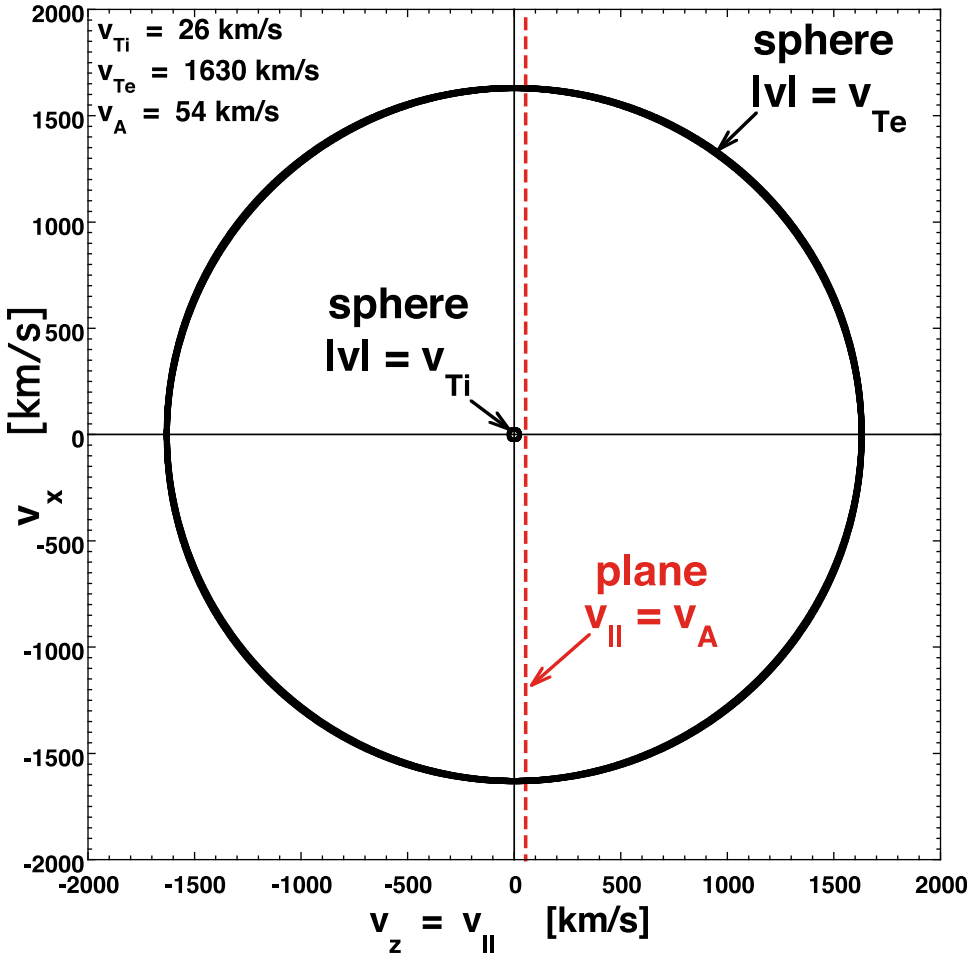

Figure 2. In $v_{\|} - v_{\perp}$ space, a sphere at $|\underline{v}| = v_{Ti}$ (inner circle), a sphere at $|\underline{v}| = v_{Te}$ (outer circle), and the $v_{\|} = v_{\|}$ resonance plane (red).

For electrons in the Alfvén speed resonance plane with $v_{\|} \approx v_A$, we would like to know the time required for Coulomb collisions to scatter the electron out of the resonance.

[12] In Figure 3 the geometry of the scattering calculation is shown in $v_{\|} - v_{\perp}$ space. The initial velocity vector of a delta function element of the electron velocity distribution function is shown as the black vector. Note that $v_{\|} = v_A$ initially. As an example, the time for the electrons to come out of the Alfvén speed resonance will be taken to be the time scale for the electrons to random walk a distance of Fv_A in $v_{\|}$, where F is a fraction. For F = 0.1, the planes of $v_A + 0.1\ v_A$ and $v_A - 0.1\ v_A$ are shown in blue in Figure 3, and one such velocity vector after the random walk is shown in green. The random walk giving $\Delta v_{\|} = Fv_A$ can be represented by a random walk in the direction of the velocity vector by an angle $\Delta\theta$. In Figure 3, the black and green vectors (with the same lengths) are separated by a vector Δv that has length $\Delta v = Fv_A/\cos(\alpha)$. Thus, the angle $\Delta\theta$ between the black and green vectors is $\Delta\theta = \Delta v/v = Fv_A/v\cos(\alpha)$. By examining Figure 3 one finds that $\cos(\alpha) = v_{\perp}/v$, so

$$\Delta\theta = Fv_A/v_{\perp}, \tag{7}$$

which is valid for $v_{\perp} > v_A$. Taking "90°" to be 1 rad, with expression (7) for $\Delta\theta$ expression (6) becomes

$$\tau_{\Delta\theta} = \tau_{90}(Fv_A/v_{\perp})^2, \tag{8}$$

where τ_{90} in expression (8) is the electron-ion 90° random walk time at velocity v.

[13] For electron velocities larger than v_{Ti}, the electron-ion 90° Coulomb scattering time varies as v^3 [*Neufeld and Ritchie*, 1955]. Hence, we can write

$$\tau_{90}(v) = \tau_{90}(v_{Te})(v/v_{Te})^3. \tag{9}$$

Using expression (9), taking $v \approx v_{\perp}$, and using the definition $\tau_{90}(v_{Te}) = \tau_{ei}$, expression (8) becomes

$$\tau_{\Delta\theta} = F^2\ \tau_{ei}\ v_{\perp}v_A^2/v_{Te}^3. \tag{10}$$

For the typical solar wind parameters of Table 1 expression (10) becomes

$$\tau_{\Delta\theta} = 1.3 \times 10^{-2}\ \mathrm{sec}\ F^2(v_{\perp}/1\ \mathrm{km/sec}). \tag{11}$$

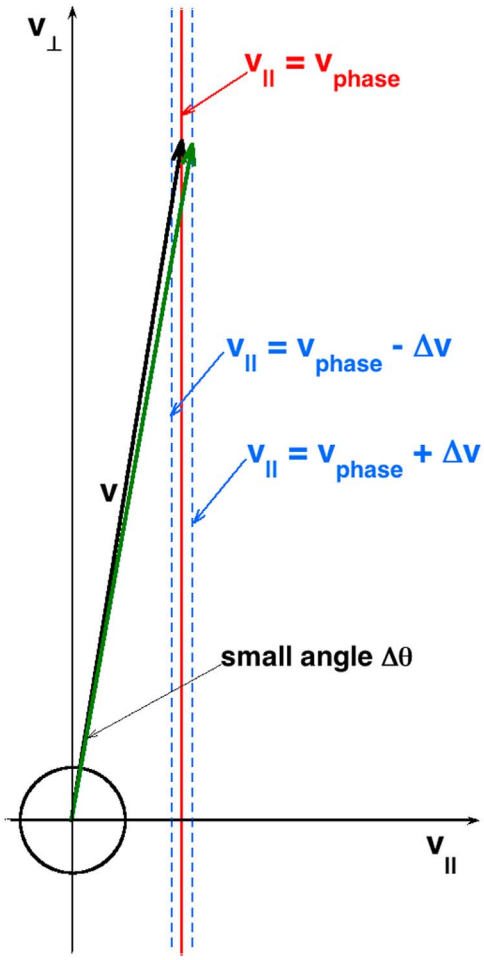

Figure 3. In $v_{\|} - v_{\perp}$ space, the angular diffusion of an electron at velocity $\underline{v}$ (black vector) out of the $v_{\|} = v_{ph}$ resonance (green vector) is depicted. (The black circle is the $|\underline{v}| = v_{Ti}$ sphere.)

For F = 0.1 and F = 1, expression (10) is plotted in Figure 4 as the two diagonal solid curves labeled "angular scattering." As can be seen, the time scales for electrons to random walk away from the $v_{\|} \approx v_A$ Landau resonance are orders of magnitude smaller than the $\tau_{ei} = 1.9 \times 10^4$ s rule-of-thumb scattering time given by expression (1).

[14] In the vicinity of $v_{\perp} = 0$, electrons are scattered out of the $v_{\|} \approx v_A$ Landau resonance by energy-scattering-type collisions with the protons rather than angular scattering collisions with the protons. The velocity diffusion of the electrons being isotropic (e.g., compare equations (6.4.8) and (6.4.9) of *Krall and Trivelpiece* [1973]), for electrons with velocities v greater than v_{Ti}, the time scale for random walking a distance Fv_A in the parallel-to-**B** direction is obtained from *Krall and Trivelpiece*'s [1973] equations (6.4.8)–(6.4.10) as

$$\tau_{\|} = m_e^2 \, v^3 \, F^2 / 8 \, \pi \, n \, e^4 \log_e(\Lambda), \qquad (12)$$

where $v = (v_A^2 + v_{\perp}^2)^{1/2}$. Using expression (1) for τ_{ei}, expression (12) is conveniently written as

$$\tau_{\|} = \left((v_A^2 + v_{\perp}^2)/v_{te}^2\right)^{3/2} F^2 \, \tau_{ei}, \qquad (13)$$

which is valid for $v_{\perp} \ll v_A$ on the resonance plane of Figure 2. For the typical solar wind parameters of Table 1, expression (13) can be written

$$\tau_{\|} = \left(2900 + v_{\perp}^2\right)^{3/2} F^2 \; 4.4 \times 10^{-6} \text{ sec}, \qquad (14)$$

with $v_{\perp}$ expressed in km/s. Expression (14) is plotted for F = 0.1 and F = 1 as the solid curves in the vicinity of $v_{\perp} = 0$ in Figure 4, labeled as "forward-backward." In Figure 4, dashed curves are generated that connect the slowing-down (foreward-backward) calculations valid for $v_{\perp} \ll v_A$ to the angular scattering calculations that are valid for $v_{\perp} > v_A$. The method of generating the dashed curves is explained in section 4.

[15] The curves in Figure 4 should approximate the electron-ion scattering time for electrons to be scattered out of the Landau resonance at $v_{\|} \approx v_A$. As can be seen in Figure 4, the time scales to collisionally diffuse electrons away from the $v_{\|} = v_A$ resonance are quite fast, 10^{-2}–10^1 s. This is much faster than the periods of Alfvén waves in the solar wind, which are limited to periods below the ion cyclotron period $\tau_{ci} = 2\pi/\omega_{ci} \sim 10$ s.

[16] In sections 3 and 4, more detailed comparisons between electron-ion Coulomb collision times and wave

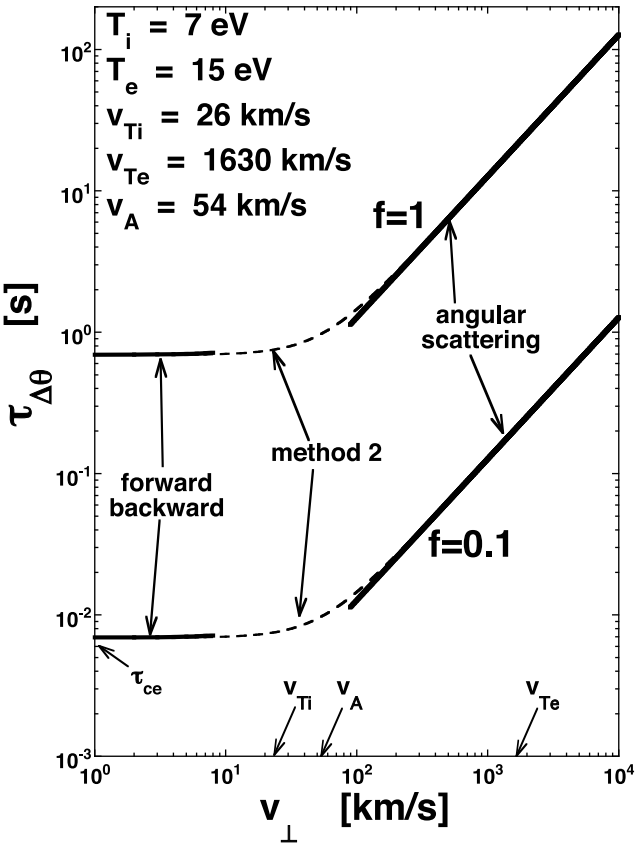

Figure 4. For the parameters of the solar wind at 1 AU, the time scale for an electron to be diffused out of the $v_{\|} = v_A$ Landau resonance is plotted as a function of $v_{\perp}$ in the resonance. The top curve (f = 1) is for a resonance of width $\pm v_A$, and the bottom curve (f = 0.1) is for a resonance of width $\pm 0.1 v_A$.

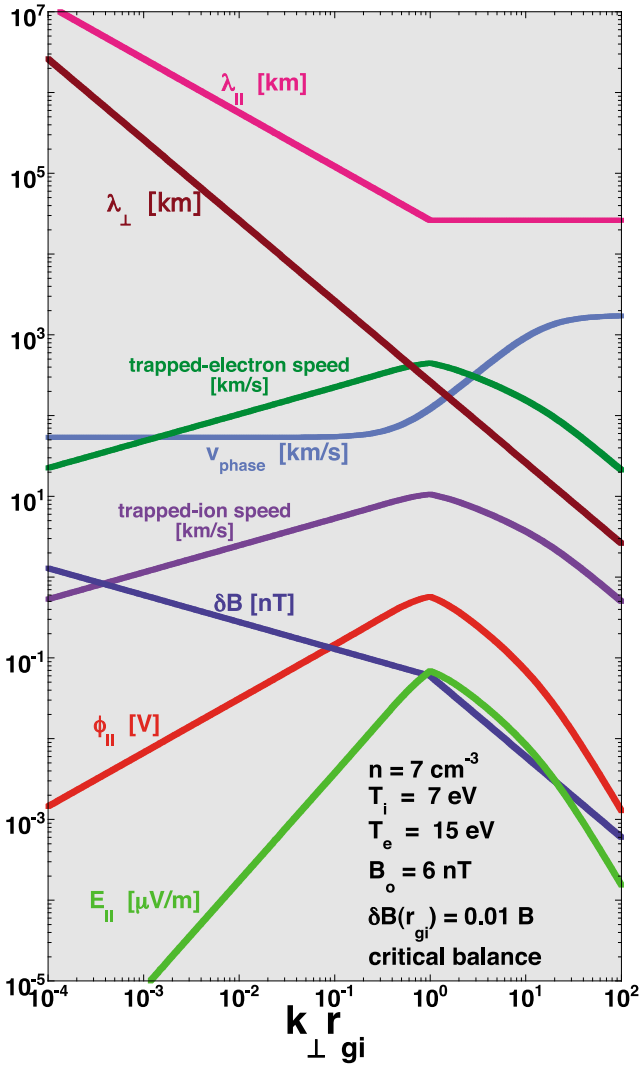

Figure 5. For Alfvén waves in the solar wind at 1 AU, a number of quantities are plotted as functions of $k_\perp$. The amplitudes of the Alfvén waves as a function of $k_\perp$ are taken to be the dark blue curve (see expressions (15a) and (15b)).

time scales will be made for Alfvén waves in the solar wind at 1 AU.

3. Parallel Electric Fields and the Electrostatic Potentials of Alfvén Waves

[17] Following the fluid treatment of *Hollweg* [1999], the properties of the parallel electric fields of Alfvén waves will be estimated. Later in section 3, numerical solutions of the linear Vlasov equation will be used to obtain more accurate estimates. For a low-amplitude MHD turbulence spectrum for the solar wind at 1 AU in which the fluctuation amplitude is $\delta B = 0.01\ B_o$ at $k_\perp r_{gi} = 1$ (John Podesta, private communication, 2010) [cf. *Podesta and Borovsky*, 2010, Figure 3], where r_{gi} is the thermal ion gyroradius $r_{gi} = v_{Ti}/\omega_{ci}$. Various Alfvén wave quantities are plotted in Figure 5 as functions of $k_\perp r_{gi}$ where the amplitude is $\delta B = 0.01\ B_o$ at $k_\perp r_{gi} = 1$. For the Alfvén wave amplitudes, $\delta B \propto k_\perp^{-1/3}$ is taken for $k_\perp r_{gi} \le 1$ and $\delta B \propto k_\perp^{-1}$ is taken for $k_\perp r_{gi} \ge 1$. This is written

$$\delta B = 0.01\ B_o \left(k_\perp r_{gi}\right)^{-1/3} \text{ for } k_\perp r_{gi} \le 1 \qquad (15a)$$

$$\delta B = 0.01\ B_o \left(k_\perp r_{gi}\right)^{-1} \text{ for } k_\perp r_{gi} \ge 1 \qquad (15b)$$

and plotted as the dark blue curve in Figure 5. The $\delta B \propto k_\perp^{-1/3}$ amplitudes correspond to a Kolmogorov $k^{-5/3}$ energy spectrum in the "inertial subrange," and the $\delta B \propto k_\perp^{-1}$ amplitudes correspond to a steeper k^{-3} energy spectrum in the "dissipation range" or "kinetic range" [cf. *Leamon et al.*, 1998; *Smith et al.*, 2006; *Alexandrova et al.*, 2009; *Sahraoui et al.*, 2009, 2010]. For convenience it will be assumed that the functional form of the velocity (= electric field) spectrum of the solar wind is the same as the functional form of the magnetic field spectrum, which is in fact not really true for the inertial subrange: The velocity spectra tends to have a shallower spectral index than the magnetic field, and the energy density of the magnetic field fluctuations exceeds the energy density of the velocity fluctuations [cf. *Podesta et al.*, 2007; *Roberts*, 2010; *Podesta*, 2011; J. E. Borovsky, The velocity and magnetic field fluctuations of the solar wind at 1 AU: Statistical analysis of Fourier spectra, unpublished manuscript, 2011; S. Boldyrev et al., Spectral scaling laws in MHD turbulence simulations and in the solar wind, submitted to *Physical Review Letters*, 2011].

[18] For most of the Alfvén wave quantities of interest here, a value of $k_\parallel$ is needed. Calculations will be done on the critical balance curve [*Goldreich and Sridhar*, 1997] $k_\parallel = k_\parallel(k_\perp)$. This curve is obtained by equating the wave-crossing time $\tau_{wave} = \lambda_\parallel/v_{ph} = 2\pi/k_\parallel v_{ph}$ with the eddy turnover time $\tau_{eddy} = \lambda_\perp/\delta v_\perp = 2\pi/k_\perp \delta v_\perp$, where v_{ph} is the parallel-to-$\vec{B}$ phase velocity of the wave and $\delta v_\perp$ is the velocity amplitude of the wave. This gives

$$k_\parallel/k_\perp = \delta v_\perp/v_{ph}. \qquad (16)$$

The wave velocity perturbation $\delta v_\perp$ is an $\mathbf{E} \times \mathbf{B}$ drift in the wave electric field $\delta E_\perp$, so $\delta v_\perp = c\delta E_\perp/B$. The wave electric field $\delta E_\perp$ is related to the wave magnetic field δB by $\delta E_\perp/\delta B = v_{ph}/c$. This last relation means that $\delta v_\perp = v_{ph}\delta B/B$. With this, expression (16) for the critical balance curve becomes

$$k_\parallel/k_\perp = \delta B/B_o. \qquad (17)$$

The wavelengths $\lambda_\perp = 2\pi/k_\perp$ and $\lambda_\parallel = 2\pi/k_\parallel$ are plotted as the dark red and the pink curves in Figure 5.

[19] *Hollweg*'s [1999] equation (25) expresses the phase velocity along the magnetic field $v_{ph} = \omega/k_\parallel$ of the Alfvén wave as

$$v_{ph} = v_A\left(1 + k_\perp^2 C_s^2/\omega_{ci}^2\right)^{1/2}\left(1 + k_\perp^2 c^2/\omega_{pe}^2\right)^{-1/2}, \qquad (18)$$

where $v_A = B_o/(4\pi n m_i)^{1/2}$ is the Alfvén speed and C_s/ω_{ci} is an ion-acoustic gyroradius, with the ion-acoustic speed being $C_s = ((\gamma_i k_B T_i + \gamma_e k_B T_e)/m_i)^{1/2}$ and the ion cyclotron frequency being $\omega_{ci} = eB_o/m_i c$. We will take $\gamma_i = 5/3$ and $\gamma_e = 1$ [e.g., *Nicholson*, 1983, section 7.5]. For the typical solar wind parameters of Table 1, expression (18) for the

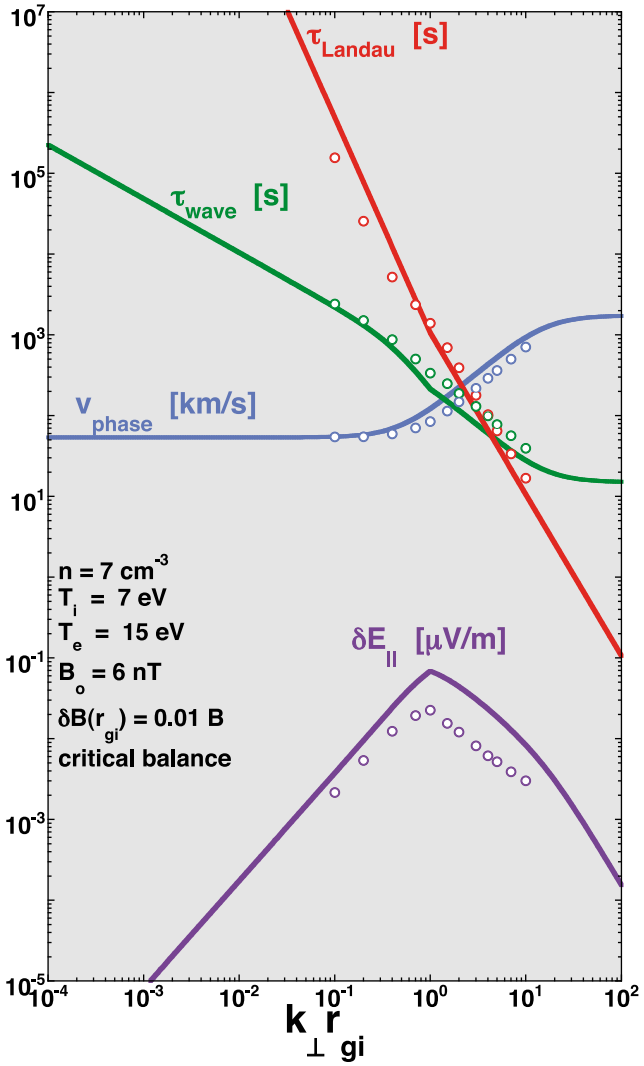

Figure 6. For Alfvén waves in the solar wind at 1 AU, several critical properties are plotted as the solid curves from fluid calculations and as open circles from linear Vlasov solutions.

phase velocity v_{ph} is plotted as a function of $k_\perp r_{gi}$ as the light blue curve in Figure 5. As can be seen, for $k_\perp \ll r_{gi}^{-1}$ the parallel phase velocity v_{ph} is at the Alfvén speed v_A = 54 km/s. This is the fluid or MHD range of wave numbers where the shear Alfvén wave is dispersionless [*Gary and Borovsky*, 2008]. As $k_\perp$ approaches r_{gi}^{-1}, the phase velocity begins to increase above v_A, and for $k_\perp > r_{gi}^{-1}$ there is strong dispersion to the mode. In this range of wave numbers the mode is known as the kinetic Alfvén wave [cf. *Hasegawa and Chen*, 1976; *Hasegawa*, 1977; *Goertz*, 1984; *Lysak and Lotko*, 1996; *Gary and Nishimura*, 2004]. For simplicity, we will refer to the mode in both ranges of wave numbers as the Alfvén wave.

[20] If δB is the magnetic field amplitude of the Alfvén wave, then the perpendicular electric field $\delta E_\perp$ of the wave is [*Hollweg*, 1999, equation (2)]

$$\delta E_\perp = (v_{ph}/c)\delta B. \tag{19}$$

Hollweg's equation (23) expresses the parallel electric field $\delta E_\parallel$ of the Alfvén wave in terms of the perpendicular electric field $\delta E_\perp$ as

$$\delta E_\parallel = \delta E_\perp \left[(m_e/m_i)v_A^2 - \gamma_e(T_e/T_i)v_{ti}^2\right]k_\perp k_\parallel\, \omega_{ci}^{-2}\left(1+\gamma_i k_\perp^2 r_{gi}^2\right)^{-1}. \tag{20}$$

Unless $\beta_e \le 2\, m_e/m_i$, which is unlikely for the solar wind, the inertial-Alfvén-wave term $(m_e/m_i)v_A^2$ in the square bracket of expression (20) is ignorable. Ignoring this term and using expression (19) for $\delta E_\perp$ and then expression (18) for v_{ph}, expression (20) becomes

$$\delta E_\parallel = \delta B (v_A/c)(T_e/T_i)(k_\parallel/k_\perp)\gamma_e k_\perp^2 r_{gi}^2\left(1+\gamma_i k_\perp^2 r_{gi}^2\right)^{-1} \times \left(1+k_\perp^2 C_s^2/\omega_{ci}^2\right)^{1/2}\left(1+\gamma_i k_\perp^2 c^2/\omega_{pe}^2\right)^{-1/2}. \tag{21}$$

For the typical solar wind parameters of Table 1, and taking $k_\parallel$ from expression (17) and δB from expressions (15), the parallel electric field $E_\parallel$ given by expression (21) is plotted as a function of $k_\perp r_{gi}$ as the light green curve in Figure 5.

[21] If the parallel electric field of a wave varies as $E_\parallel(z) = \delta E_\parallel \sin(k_\parallel z)$, where z is the direction along $\vec{B}_o$, then the electrostatic potential $\phi = \int E_\parallel\, dz$ varies as $\phi(z) = (\delta E_\parallel/k_\parallel)\cos(k_\parallel z)$ and the maximum potential difference within the wave is

$$\phi_\parallel = 2\delta E_\parallel/k_\parallel = \lambda_\parallel\, \delta E_\parallel/\pi. \tag{22}$$

Using expression (21) for $\delta E_\parallel$ in expression (22), the electrostatic potential of the Alfvén wave is

$$\phi_\parallel = 2\,\delta B\, r_{gi}(v_A/c)(T_e/T_i)\gamma_e k_\perp r_{gi}\left(1+\gamma_i k_\perp^2 r_{gi}^2\right)^{-1} \times \left(1+k_\perp^2 C_s^2/\omega_{ci}^2\right)^{1/2}\left(1+\gamma_i k_\perp^2 c^2/\omega_{pe}^2\right)^{-1/2}. \tag{23}$$

Note that $\phi_\parallel$ is independent of $k_\parallel$ and of $k_\parallel/k_\perp$. For the typical solar wind parameters of Table 1, expression (23) is plotted as the red curve in Figure 5. At long wavelengths (low $k_\perp$) the potential $\phi_\parallel$ of the wave increases linearly with $k_\perp$ even though the wave amplitude δB decreases with increasing $k_\perp$. In the "dissipation range" the potential $\phi_\parallel$ of the wave decreases with increasing $k_\perp$.

[22] For comparison with the fluid calculations of this section, the linear Vlasov-Maxwell dispersion relation is computationally solved without approximation [cf. *Gary and Borovsky*, 2004; *Podesta et al.*, 2010] to discern the properties of Alfvén waves and kinetic Alfvén waves. The plasma parameters of Table 1 are used with $\delta B_\perp$ of the Alfvén waves given as a function of $k_\perp$ on the critical balance curve by expression (15) and $k_\parallel$ given as a function of $k_\perp$ by expression (17). In the $k_\perp \gg k_\parallel$ regime where the Vlasov calculations will be performed, damping via the Landau resonance is much stronger than cyclotron damping [*Gary and Borovsky*, 2004]. Note that in the Vlasov calculations damping via the Landau resonance includes Landau damping off the parallel electric field and transit time damping off the compressional magnetic field (see sections 5 and 6.3). In Figure 6 the parameters $\tau_{wave} = 2\pi/\omega_{real}$, $\tau_{Landau} = 1/\omega_{imag}$, v_{ph}, and $\delta E_\parallel$ are plotted as points from the linear Vlasov solutions

where they are compared with τ_{wave}, v_{ph}, and $\delta E_{\parallel}$ from *Hollweg*'s [1999] fluid approach used throughout this section and with τ_{Landau} from *Gary and Borovsky*'s [2008] parameterization for electron Landau damping (with $A \approx 0.6$). The focus of the linear Vlasov solutions is on the transition from the MHD regime to the kinetic regime: $k_{\perp} r_{gi} = 0.1$–10. As can be seen in Figure 6, *Hollweg*'s [1999] fluid treatment does a good job of describing the properties of the Alfvén waves from the MHD regime into the kinetic-Alfvén-wave regime. Also, the *Borovsky and Gary* [2009] (see also *Gary and Borovsky* [2008]) long-wavelength parameterization of the Alfvén wave Landau-damping rate (red curve in Figure 6) holds well into the kinetic-Alfvén-wave regime $k_{\perp} > r_{gi}^{-1}$.

4. Coulomb Scattering Disrupting Distribution Function Evolution

[23] For Coulomb collisions to disrupt plateau formation on the electron distribution function, electrons must be diffused out of the Landau resonance by collisions in a diffusion time τ_d that is comparable to or shorter than the trapped-electron bounce time τ_b [cf. *Auerbach*, 1977; *Kaganovich*, 1999; *Bilato and Brambilla*, 2004, 2008]. The distance $\Delta v_{\parallel}$ in $v_{\parallel}$ that an electron must be diffused is given by the kinetic energy (in the wave frame) of electrons that are trapped by the wave potential $\phi_{\parallel}$. The maximum parallel-to-$\vec{B}_o$ kinetic energy $m_e \Delta v_{\parallel}^2/2$ that can be trapped in the wave's potential well $e\phi_{\parallel}$ gives

$$\Delta v_{\parallel} = \left(2e\phi_{\parallel}/m_e\right)^{1/2} \tag{24}$$

for the width of the Landau resonance. Using expression (23) for $\phi_{\parallel}$, expression (24) is plotted as the green curve for electrons in Figure 5 and as the purple curve for protons (with m_i replacing m_e in expression (24)). Note that since $\phi_{\parallel}$ is independent of the wave number anisotropy $k_{\parallel}/k_{\perp}$, the trapping velocity $\Delta v_{\parallel}$ is independent of the anisotropy.

[24] The bounce time (= bounce period) τ_b for an electron in a wave with electric field $E_{\parallel}$ is

$$\tau_b = 2\pi\left(m_e/eE_{\parallel}k_{\parallel}\right)^{1/2} = 2\pi\left(2m_e/e\phi_{\parallel}k_{\parallel}^2\right)^{1/2}, \tag{25}$$

where $\phi_{\parallel} = 2E_{\parallel}/k_{\parallel}$ was used. For $k_{\parallel}$ given by expression (17) and $\phi_{\parallel}$ given by expression (23), the bounce time given by expression (25) is plotted as the dark green curve in Figure 7. Also plotted for comparison in Figure 7 is the wave period $\tau_{wave} = 2\pi/\omega_{real} = 2\pi/v_{ph}k_{\parallel}$ in red. The horizontal dashed lines in Figure 7 represent the proton gyroperiod τ_{ci}, the electron-ion scattering time τ_{ei} (from expression (1)), the electron-electron scattering time τ_{ee}, and the ion-ion scattering time τ_{ii}. A resistive-damping time scale $\tau_{resistive}$ (defined below) is plotted in light green. An analytic expression for the Landau-damping time scale $\tau_{Landau} = 1/\omega_{imag}$ of Alfvén waves [*Borovsky and Gary*, 2009, equation (19)] valid in the long-wavelength limit is

$$\tau_{L\,B+G} = 1/\gamma = A^{-1}\,\omega_{pe}^{-1}\left(k_{\parallel}\lambda_{De}\right)^{-1}\left(k_{\perp}c/\omega_{pe}\right)^{-2}, \tag{26}$$

where λ_{De} is the Debye length. With the constant $A \approx 0.6$ for electron Landau damping, the damping time $\tau_{L\,B+G}$ given by

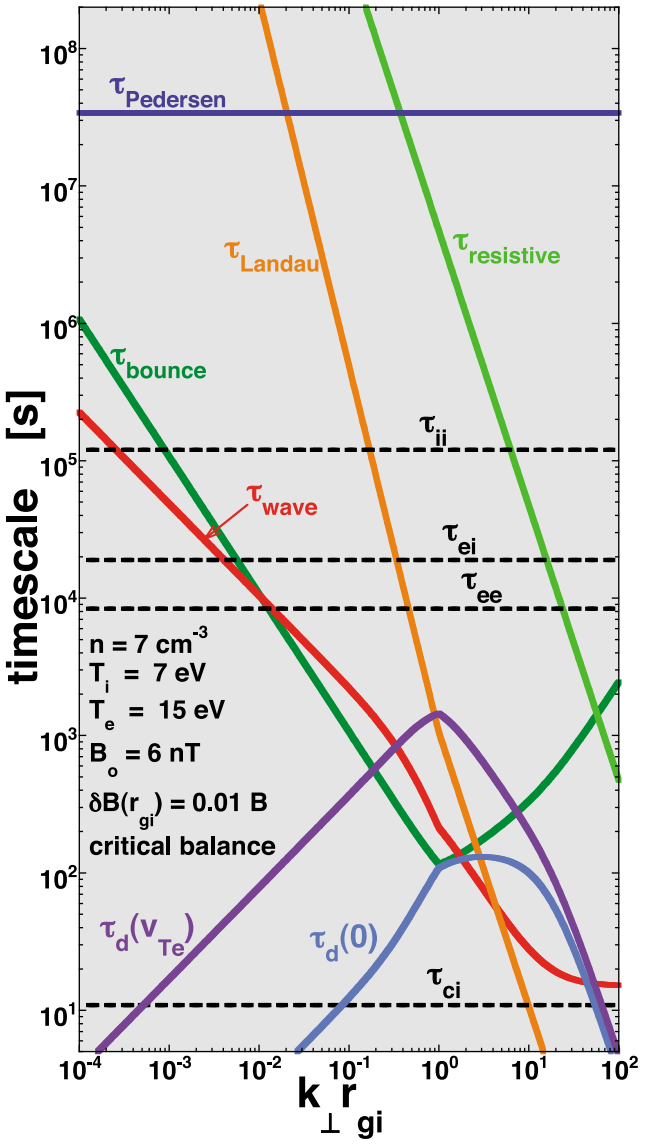

Figure 7. For Alfvén waves in the solar wind at 1 AU, a number of time scales are plotted as functions of $k_{\perp}$. The amplitudes of the Alfvén waves as a function of $k_{\perp}$ (which controls the bounce time as a function of $k_{\perp}$) are given by expressions (15a) and (15b).

expression (26) is plotted as the orange curve in Figure 7. The diffusion of the electron velocity distribution function in velocity space goes according to

$$\partial f/\partial t = D\,\partial^2 f/\partial v^2, \tag{27}$$

where the diffusion coefficient $D = D(v)$ for electron-ion Coulomb scattering is a function of electron velocity v in the proton's frame. For velocity $v = v_{Te}$, the diffusion coefficient in expression (27) is $D(v_{Te}) = v_{Te}^2/\tau_{ei}$, which is the definition of τ_{ei}. Expression (1) for τ_{ei} can be rewritten $\tau_{ei} = \gamma\, v_{Te}^3$ where $\gamma \equiv m_e^2/8\,\pi\,n\,e^4\,\log_e(\Lambda)$. With this expression for τ_{ei}, the diffusion coefficient $D(v_{Te}) = v_{Te}^2/\tau_{ei} = 1/\gamma v_{Te}$. Hence, at any electron velocity v the diffusion coefficient is $D(v) = 1/\gamma v$.

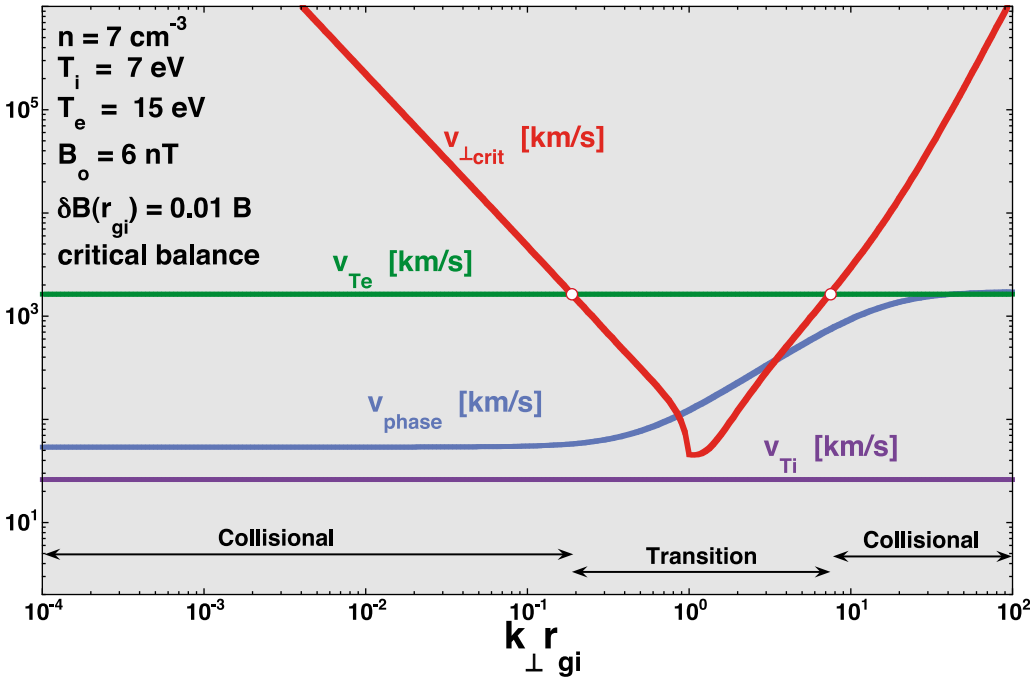

Figure 8. For Alfvén waves in the solar wind at 1 AU, $v_{\perp crit}$ is plotted as a function of $k_\perp$ and compared with v_{Te}. The amplitudes of the Alfvén waves as a function of $k_\perp$ are given by expressions (15a) and (15b).

Using $\gamma = \tau_{ei}/v_{Te}^3$, the diffusion coefficient is conveniently written

$$D(v) = v_{Te}^3/\tau_{ei}v. \tag{28}$$

With expression (28), expression (27) gives the diffusion time $\tau_d(v, \Delta v_\parallel)$ to random walk a velocity $\Delta v_\parallel$ at velocity v as

$$\tau_d(v, \Delta v_\parallel) = \Delta v_\parallel^2/D(v) = \tau_{ei}(\Delta v_\parallel)^2 v/v_{Te}^3. \tag{29}$$

For $\Delta v_\parallel = v_A$ and $\Delta v_\parallel = 0.1\ v_A$, expression (29) was used to plot τ_d as a function of $v_\perp$ along the $v_\parallel = v_A$ resonance as the two dashed curves in Figure 4 labeled "method 2," with $v = (v_\perp^2 + v_A^2)^{1/2}$ in expression (29). As can be seen by comparing the dashed curves with the solid curves, the generalized calculation of the velocity diffusion (expression (35)) agrees with the angular diffusion derivation in section 2 and with the forward-backward derivation in section 2.

[25] Using expression (24) for $\Delta v_\parallel$, expression (29) becomes

$$\tau_d = 2e\phi_\parallel \tau_{ei} v/m_e v_{Te}^3 \tag{30}$$

for the diffusion time on the resonance plane. Expressing the velocity v on the $v_\parallel = v_{ph}$ resonance plane as $v = (v_\perp^2 + v_{ph}^2)^{1/2}$, expression (30) becomes

$$\tau_d = 2e\phi_\parallel \tau_{ei}\left(v_\perp^2 + v_{ph}^2\right)^{1/2}/m_e v_{Te}^3 \tag{31}$$

for $v_\perp$ on the plane. In Figure 7 the Coulomb scattering diffusion time τ_d given by expression (31) is plotted for $v_\perp = 0$ (blue curve labeled $\tau_d(0)$) and for $v_\perp = v_{Te}$ (purple curve labeled $\tau_d(v_{Te})$). As can be seen by examining the blue and purple curves, except in the region where $k_\perp \sim r_{gi}^{-1}$, the diffusion times $\tau_d(v_{Te})$ and $\tau_d(0)$ are very much faster than the wave time scales τ_{wave} and the trapped-electron bounce times τ_b.

[26] For plateau formation to be impeded by the Coulomb scattering of trapped electrons, it is required that the diffusion time τ_d be less than or equal to the bounce time τ_b, written $\tau_d \le \tau_b$. With expression (25) for τ_b and expression (30) for τ_d, the relation $\tau_d \le \tau_b$ for prevention of plateau formation can be written as

$$v_\perp \le v_{\perp crit}, \tag{32}$$

where the critical velocity $v_{\perp crit}$ is

$$v_{\perp crit} = \left[2\pi^2\left(v_{Te}^2 m_e/e\phi_\parallel\right)^3 \tau_{ei}^{-2}k_\parallel^{-2} - v_{ph}^2\right]^{1/2}. \tag{33}$$

With the wave electrostatic potential $\phi_\parallel$ given by expression (23), for the typical solar wind parameters of Table 1 the critical velocity $v_{\perp crit}$ of expression (33) is plotted as the red curve in Figure 8.

[27] On the resonance plane of Figure 2, electrons with $v_\perp < v_{\perp crit}$ are scattered out of the trapping resonance faster than their bounce time. Hence, regions of the resonance plane with $v_\perp < v_{\perp crit}$ will not experience plateau formation. Electrons on the resonance plane with $v_\perp > v_{\perp crit}$ are "collisionless" and regions of the resonance plane with $v_\perp > v_{\perp crit}$ can experience plateau formation. Depending on the value of $v_{\perp crit}$, electron-ion Coulomb collisions will be important or ignorable for the Landau-damping problem. Three regimes of $v_{\perp crit}$ can be envisioned.

4.1. Regime I: $v_{\perp crit} \gg v_{Te}$

[28] In this regime, essentially all of the electrons on the $v_{\parallel} = v_{ph}$ resonance plane of Figure 2 are collisional, plateau formation is disrupted, and the electron distribution function remains Maxwellian in the vicinity of the $v_{\parallel} = v_{ph}$ resonance. Electron Landau damping occurs (although, owing to trapping, it may occur at a rate other than that given by the linear Vlasov calculations). In addition, a resistive damping of the Alfvén wave occurs because of a dissipative Pedersen current driven by $\delta E_{\perp}$ of the wave owing to the nonzero Pedersen conductivity σ_P of the solar wind. *Borovsky*'s [1993] equation (A4) gives the *e*-folding time scale of the damping to be $\tau_{Ped} = c^2/4\pi v_A^2 \sigma_P$. For a fully ionized plasma with $\tau_{ei} \ll \tau_{ce}$ the Coulomb-scattering-produced Pedersen conductivity σ_P is [cf. *Mitchner and Kruger*, 1973, p. 424] $\sigma_P = ne^2/m_e \omega_{ce}^2 \tau_{ei}$. (For the typical solar wind parameters of Table 1, this is $\sigma_P = 7.2 \times 10^{-2}$ s^{-1}.) Using this expression for σ_P, the Pedersen damping time becomes

$$\tau_{Ped} = (m_e/m_i)\left(c^4/v_A^4\right)/16\pi^2\tau_{ei}. \quad (34)$$

[29] For the parameters of Table 1, expression (34) becomes $\tau_{Ped} = 3.4 \times 10^7$ s = 1.1 yr, which is plotted as the dark blue curve in Figure 7. Additionally, a resistive damping of Alfvén waves occurs owing to electron-ion Coulomb collisions resistively dissipating field-aligned currents associated with $E_{\parallel}$ [*Borovsky*, 1993; *Lessard and Knudsen*, 2001]. The resistive damping time scale for Alfvén waves is given by equation (A5) of *Borovsky* [1993]: $\tau_{resistive} = 4\pi\sigma_{\parallel}/c^2 k_{\perp}^2$. For a parallel-to-B electric conductivity $\sigma_{\parallel} = ne^2\tau_{ei}/m_e$ (compare section 4.3.3 of work by *Alfvén and Falthammar* [1963] or equation (12.4.6) of *Bostrom* [1973]), this is

$$\tau_{resistive} = \left(k_{\perp}^2 c^2/\omega_{pe}^2\right)^{-1}\tau_{ei}. \quad (35)$$

For the typical solar wind parameters of Table 1, the resistive damping time given by expression (35) is plotted as the light blue curve in Figure 7. *Bilato and Brambilla* [2004, 2008] argue that within regime I, if $\tau_d < \tau_{wave}$, then the Landau-damping rate will be collisionally lowered because the duration of wave-particle interactions is governed by the collision time, with a shorter collision time meaning a shorter interaction time and a weaker Landau damping. A counterargument to this is that the Landau-damping rate is not altered by collisions because for every electron knocked out of resonance another electron is knocked in, and the Maxwellian phase space is continuously populated and the Landau damping is unimpeded.

4.2. Regime II: $v_{Te} > v_{\perp crit} > 0$

[30] In this regime a fraction of the electrons on the $v_{\parallel} = v_{ph}$ resonance plane of Figure 2 are collisional, the slower electrons. In this regime, trapping occurs for the high-$v_{\perp}$ electrons and plateau formation can occur in the high-$v_{\perp}$ portions of the resonance plane. The low-$v_{\perp}$ portion is collisional and the electron distribution function remains locally Maxwellian on this portion. Linear Landau damping is reduced owing to a reduction in the number of electrons at the resonance that participate in the damping.

4.3. Regime III: $v_{\perp crit} \le 0$

[31] In this regime, none of the electrons on the $v_{\parallel} = v_{ph}$ resonance plane of Figure 2 are collisional, trapping occurs for all regions of the resonance plane, and plateau formation can occur for all regions of the resonance plane. Landau damping can be turned off owing to plateau formation flattening the electron velocity distribution function at the Landau resonance.

[32] As can be seen in Figure 8, for the spectrum of Alfvén waves chosen to match the spectrum of magnetic field fluctuations in the solar wind, $v_{\perp crit}$ (red curve) is greater than v_{Te} (green curve) for most values of $k_{\perp}$. This is representative of regime I above. Hence, for most $k_{\perp}$ values, Coulomb collisions maintain the Maxwellian distribution at the Alfvén wave resonance, no plateau formation occurs, and Landau damping persists indefinitely. For about a decade of $k_{\perp}$ around $k_{\perp} r_{gi} = 1$, the critical velocity $v_{\perp crit}$ is less than v_{Te} but greater than zero: This is representative of regime II above. For $k_{\perp}$ values around r_{gi}^{-1} the Maxwellian is maintained only for the low-$v_{\perp}$ electrons in the resonance, and the faster electrons are subject to plateau formation. Here Landau damping by the faster electrons can be reduced, but Landau damping by the lower-energy electrons persists indefinitely. Around $k_{\perp} = r_{gi}^{-1}$ the total amount of Landau damping is reduced, but that reduced level persists indefinitely.

[33] In Figure 9 (top) the calculations are repeated for parameters typical of fast wind (blue) and for parameters typical of slow wind (purple), and the $v_{\perp crit}$ curve for the two cases is plotted and compared with v_{Te} (green). The fast-wind and slow-wind parameters used are from two corotating interaction region (CIR) collections utilized for superposed-epoch studies [*Denton and Borovsky*, 2008; *Borovsky and Denton*, 2010]. The relevant average post-CIR fast-wind parameters are $B_o = 6.9$ nT, $T_i = 26.3$ eV, and $n = 3.7$ cm^{-3}; the average pre-CIR slow-wind parameters are $B_o = 5.2$ nT, $T_i = 4.5$ eV, and $n = 8.4$ cm^{-3}. The CIR collections do not have electron temperature measurements: The electron temperature does not vary substantially with wind speed [*Skoug et al.*, 2000], so $T_e = 15$ eV is taken for both fast and slow wind. These give $v_A = 78.2$ km/s, $v_{Ti} = 50.3$ km/s, and $\tau_{ei} = 3.1 \times 10^4$ s for the fast wind and $v_A = 39.1$ km/s, $v_{Ti} = 20.8$ km/s, and $\tau_{ei} = 1.4 \times 10^4$ s for the slow wind. For the Alfvén wave amplitudes the spectrum of expression (15) is used for both the fast and the slow wind. As can be seen in Figure 9 (top) the $v_{\perp crit}$ curves are similar for fast wind, slow wind, and the typical wind parameters of Table 1. Hence, the conclusions about which regime (I, II, or III) the Landau resonance is on versus the value of $k_{\perp}$ do not vary greatly with the type of wind.

[34] In Figure 9 (bottom) the calculations are repeated with the amplitudes of the Alfvén waves varied. The typical solar wind parameters of Table 1 are used. The red curve in Figure 9 (bottom) is the $v_{\perp crit}$ curve from Figure 8 for a δB spectrum with $\delta B(k_{\perp} r_{gi} = 1) = 0.01\ B_o$ (see expressions (15a) and (15b)), which is $\lambda_{\parallel} = 100\lambda_{\perp}$ at $k_{\perp} r_{gi} = 1$ (see expression (17)); the blue curve is $v_{\perp crit}$ for a δB spectrum that is 3 times weaker and the green curve is $v_{\perp crit}$ for a dB spectrum that is 3 times stronger. As can be seen, for the blue curve corresponding to lower-amplitude Alfvén waves $v_{\perp crit}$ is greater than v_{Te} for all $k_{\perp}$ values so the Landau resonance is in regime I (collisional) for all $k_{\perp}$ values. And as can be seen, for the green curve corresponding to larger-amplitude Alfvén waves there is a region from $k_{\perp} r_{gi} \approx 0.3$ to $k_{\perp} r_{gi} \approx 30$ wherein

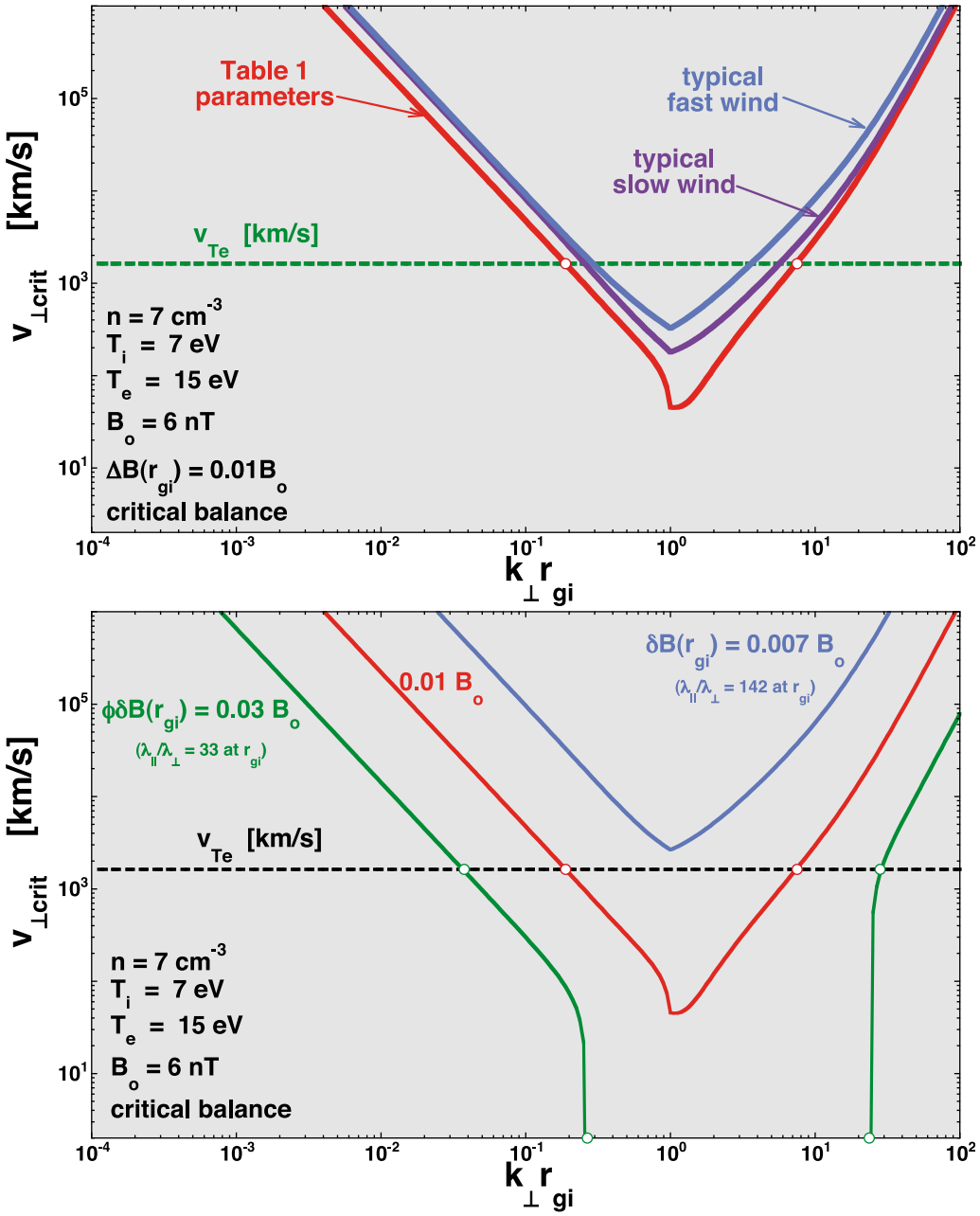

Figure 9. For Alfvén waves in the solar wind at 1 AU, curves of $v_{\perp crit}$ are plotted as functions of $k_\perp$ and compared with v_{Te}. In both plots the red curve is the $v_{\perp crit}$ curve from Figure 8. In the top plot the parameters of the solar wind are varied from typical slow wind (purple) to typical fast wind (blue). In the bottom plot the amplitudes of the Alfvén waves are varied from $B_{amp} = 0.007$ (blue curve) to $B_{amp} = 0.03$ (green curve).

the Landau resonance is collisionless (regime III) and plateau formation could turn off Landau damping.

[35] Using a series of $v_{\perp crit}$ curves as in Figure 9 (bottom), the regions of $k_\perp$ space that are collisional (regime I), collisionless (regime III), or transitional (regime II) are mapped out as a function of the amplitude of the Alfvén waves. As in expressions (15a) and (15b), the Alfvén wave amplitude spectrum is taken to be of the form $\delta B \propto k_\perp^{-1/3}$ for $k_\perp \le r_{gi}^{-1}$ and $\delta B \propto k_\perp^{-1}$ for $k_\perp \ge r_{gi}^{-1}$ with amplitude $\delta B/B_o = B_{amp}$ at $k_\perp r_{gi} = 1$. (For the earlier calculations, $B_{amp} = 0.01$ has been used; see expressions (15a) and (15b).) Figure 10 plots B_{amp} (vertical) from $B_{amp} = 0.001$ to $B_{amp} = 1$, which is $\lambda_\parallel/\lambda_\perp = 1000$ to $\lambda_\parallel/\lambda_\perp = 1$ at $k_\perp r_{gi} = 1$. As can be seen in Figure 10, at low amplitudes the Landau resonance is collisional (blue shading) for all $k_\perp$ values. Hence, for low-amplitude Alfvén waves in the solar wind, at all $k_\perp$ values the collisional diffusion time τ_d is faster than the trapped-electron bounce time τ_b for all values of $v_\perp$ in the resonance: Plateau formation in the electron distribution function will not occur and Landau damping will not be shut off. For amplitudes B_{amp} that are larger than about 5×10^{-3}, there is a region of $k_\perp$ space around $k_\perp = r_{gi}^{-1}$ where the Landau resonance is

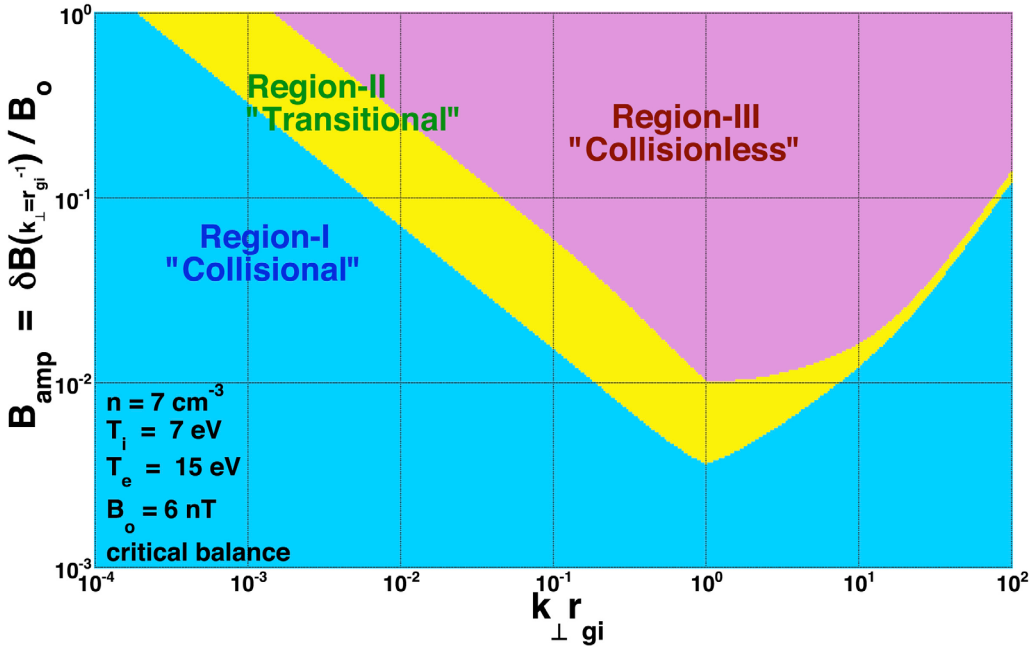

Figure 10. For Alfvén waves in the solar wind at 1 AU, the regions of $k_\perp$ where the electron Landau resonance is collisional (blue), collisionless (pink), or transitional (yellow) are plotted out as functions of the amplitude of the turbulence B_{amp}.

collisionless (pink shading in Figure 10). The larger the amplitude of the Alfvén wave, the broader this region of $k_\perp$ space is. For the observed magnetic field fluctuations of the solar wind at 1 AU, B_{amp} values of 0.01–0.05 are observed.

5. Summary: Assessment for Electron Landau Damping in the Solar Wind

[36] For low-amplitude Alfvén waves in the solar wind at 1 AU, electron-ion Coulomb collisions should prevent Landau damping from modifying the electron distribution function and electron Landau damping should persist. However, the Landau-damping rate may be other than the value given by linear Vlasov theory. For higher-amplitude Alfvén waves, there will be a region of $k_\perp$ space around $k_\perp = r_{gi}^{-1}$ where collisions are not effective in the Landau resonance and the electron distribution function may be modified away from a Maxwellian form and electron Landau damping may be shut off. However, ion Landau damping will persist.

[37] The findings of this study are summarized in the following eight points. (For points 6–8, see the discussion in sections 6 and 7.)

[38] 1. For Alfvén waves in the solar wind, the electrostatic voltages associated with the parallel electric fields of the waves are large compared with the kinetic energies of electrons at the phase velocity. As a result, the velocity range of trapped electrons is larger than the phase velocity of a wave, and the portion of the electron velocity distribution function that interacts with a wave is substantial. The resonance is so broad that electrons moving in the direction of the wave and electrons moving counter to the wave interact with the wave. In light of this broad resonance it is unclear whether linear Landau theory will accurately describe the rate of Landau damping of the solar wind Alfvén waves.

[39] 2. Trapped-electron bounce times are about equal to the wave-crossing times and eddy turnover times. Hence, the bounce times are comparable to correlation times and so trapping effects will persist in a spectrum of Alfvén waves.

[40] 3. Electron-ion Coulomb collisions will disrupt electron trapping in the Alfvén waves of the solar wind: The Coulomb scattering velocity diffusion time scales tend to be shorter than the trapped-electron bounce times.

[41] 4. Since electron-ion Coulomb collisions rapidly diffuse the velocity distribution function in the vicinity of the Landau resonance, they prevent plateau formation and maintain a Maxwellian form. This allows Landau damping to proceed indefinitely in the presence of a Maxwellian electron distribution function.

[42] 5. Electron-ion Coulomb collision rates in the solar wind are weak enough so that resistive damping by the parallel conductivity $\sigma_\parallel$ acting on $E_\parallel$ and by the Pedersen conductivity σ_P acting on $E_\perp$ can be neglected for Alfvén waves.

[43] 6. Electron transit time damping, which can dominate the linear Vlasov Landau-damping decrement at higher β values, has not been analyzed. The importance of electron trapping in the $B_\parallel$ perturbations of the Alfvén waves and the disruption of that trapping by electron-ion Coulomb collisions should be assessed.

[44] 7. Ion Landau damping associated with $E_\parallel$ and ion transit time damping associated with $B_\parallel$ have not been analyzed here for Alfvén waves in the solar wind. Specifically, the importance of ion trapping and the disruption of ion trapping by Coulomb collisions should be assessed.

[45] 8. Three cautions about calculating the Landau damping of Alfvén waves in the solar wind have been stated: (1) The wave voltages are much bigger than the energies of

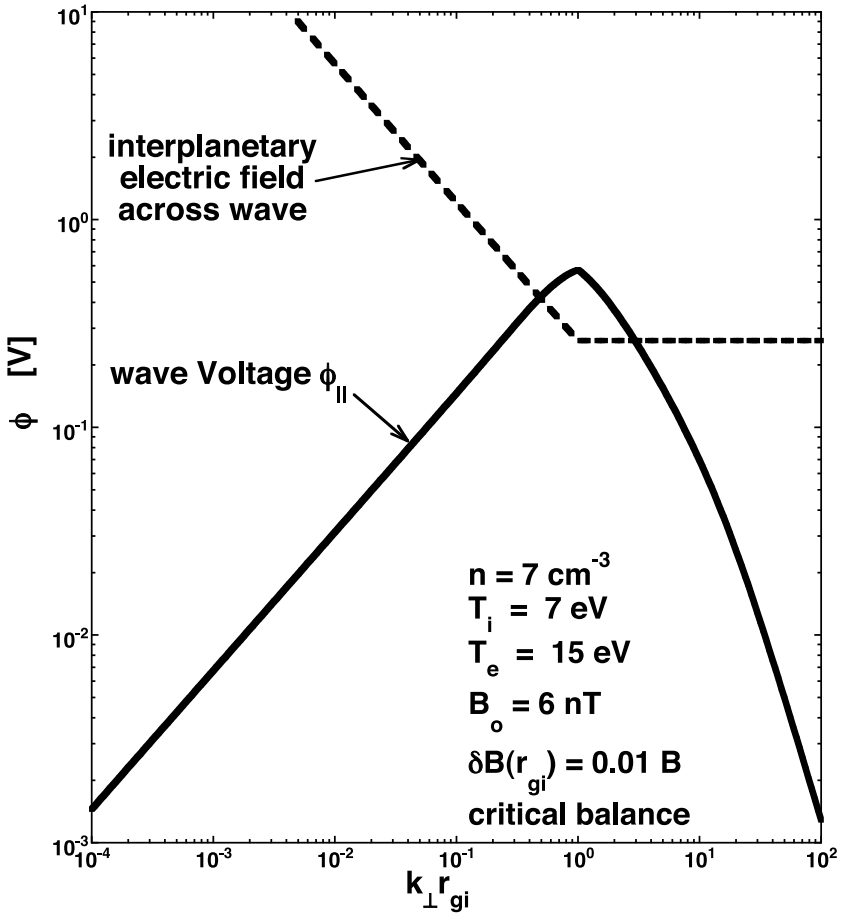

Figure 11. For Alfvén waves in the solar wind at 1 AU, the peak-to-peak electrostatic potential $\phi_{||}$ of the wave (solid curve) is compared with the potential drop of the interplanetary electric field along one-half wavelength of the wave (dashed curve).

resonant particles, and so the portion of the electron distribution function that interacts with the wave is large, requiring a Landau-damping analysis based on more than the local value of $\partial f/\partial v_{||}$ at the phase velocity. (2) Proton beams, alpha particle beams, and heavy-ion beams with velocities in the range of the Alfvén wave phase velocities should be included in any accurate analysis of the Landau damping of Alfvén waves in the solar wind. (3) Heliospheric electric fields are larger than the Alfvén wave parallel electric fields that produce the Landau damping; hence, the effects of these electric fields on the Alfvén waves and the Alfvén wave damping should be assessed.

6. Discussion 1: Other Factors Affecting Landau Damping in the Solar Wind

[46] The case of Landau damping of Alfvén waves in the solar wind is complicated by several factors, and a full assessment of the damping must account for these factors.

6.1. Solar Wind Interplanetary Electric Field

[47] There is a voltage drop in the solar wind between the Sun and the outer heliosphere. In the vicinity of 1 AU, that interplanetary electric field is observed to be manifest by a series of weak double layers, which are Debye-scale electrostatic structures. In the solar wind they are observed to have potential drops across them with average values of 4×10^{-3} V [*Mangeney et al.*, 1999; *Lacombe et al.*, 2002; *Salem et al.*, 2003] and are observed to occur about once per second in the convection past a spacecraft [*Lacombe et al.*, 2002; *Salem et al.*, 2003]. With a wind speed of 400 km/s, this is a mean electric field E_{dl} of $E_{dl} = 1 \times 10^{-5}$ V/km (pointing away from the Sun), which is on the order of the interplanetary electric field [*Lemaire and Scherer*, 1971; *Pierrard et al.*, 2001]. The field-aligned potential drops associated with weak double layers in the solar wind can be larger than the trapping potentials within the solar wind Alfvén waves, particularly for $k_{||} \ll k_\perp$ which is observed in the solar wind [*Sorriso-Valvo et al.*, 2006; *Horbury et al.*, 2008; *Podesta*, 2009; *Narita et al.*, 2010; *Wicks et al.*, 2010; *Sahraoui et al.*, 2010] and which is expected to be enhanced at higher wave numbers [*Goldreich and Sridhar*, 1997; *Boldyrev*, 2005]. For $k_{||} = k_{||}(k_\perp)$ given by critical balance, the electrical potential owed to solar wind double layers over $\lambda_{||}/2$ of an Alfvén wave is plotted as the dashed curve in Figure 11. Plotted as the solid curve for comparison is $\phi_{||}$ of the Alfvén wave from expression (26) for $\delta B(k_\perp r_{gi} = 1) = 0.01\ B_o$ (as in Figure 5). As can be seen in Figure 11, the interplanetary electric field dominates the Alfvén wave parallel electric fields until $k_\perp \sim r_{gi}$, i.e., until the Alfvén waves are

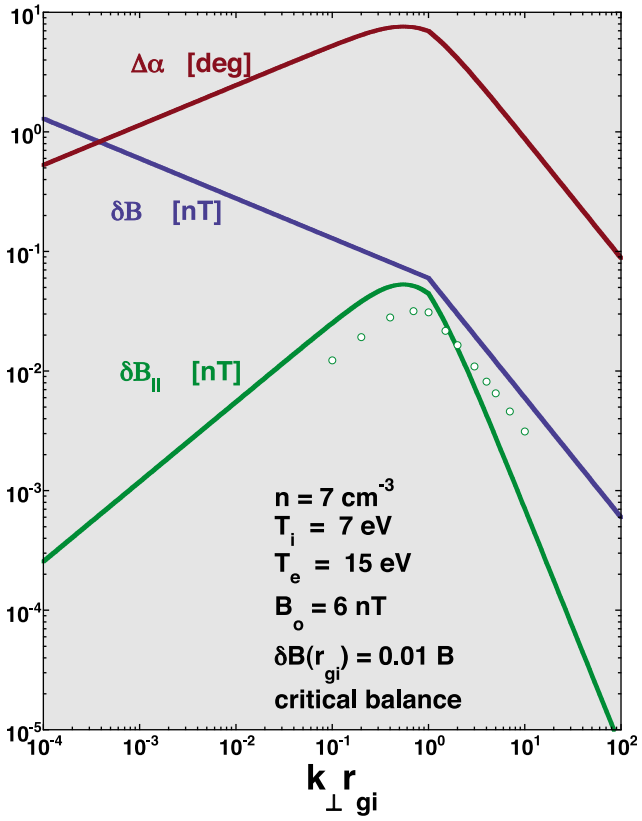

Figure 12. For Alfvén waves in the solar wind at 1 AU, the amplitude of the wave parallel magnetic field perturbation is plotted in green from fluid theory and as green circles from linear Vlasov solutions. The angular width about 90° pitch angle of the zone of magnetically mirroring particles trapped in the wave is plotted as the dark red curve.

of small enough perpendicular wavelengths to reach the kinetic range. This interplanetary electric field will modify the picture of electron trapping and nonlinear Landau damping for Alfvén waves in the solar wind. An analysis is called for.

6.2. Ion Beams Near the Landau Resonance

[48] Often in the solar wind there are proton, alpha particle, and heavy-ion beams in addition to the main proton distribution. Proton beams with sunward and antisunward parallel velocities $\sim v_A$ are common [*Feldman et al.*, 1973; *Marsch et al.*, 1982b; *Marsch*, 2006], and alpha particle beams with velocities $\sim v_A$ away from Sun relative to the main proton beam are often seen [*Asbridge et al.*, 1976; *Neugebauer and Feldman*, 1979; *Marsch et al.*, 1982a]. These beams in the vicinity of the Alfvén wave resonance need to be incorporated into the Landau-damping calculations of the Alfvén and kinetic Alfvén waves and into the distribution function evolution via waves and collisions.

6.3. Electron Transit Time Damping

[49] Alfvén waves with nonzero $k_\perp$ have a parallel electric field $\delta E_\parallel$ that enables Landau damping by ions and electrons at the $v_\parallel \approx v_A$ Landau resonance; Alfvén waves with nonzero $k_\perp$ also have a parallel magnetic field perturbation $\delta B_\parallel$ [*Hollweg*, 1999; *Gary and Borovsky*, 2008] that enables transit time damping by ions and electrons at the $v_\parallel \approx v_A$ Landau resonance. Depending on the β_i and β_e values of the plasma, the relative importance of Landau damping to transit time damping varies, with transit time damping in general becoming dominant at higher β values. *Hollweg*'s [1999] equation (28) expresses $\delta B_\parallel$ of the Alfvén wave in terms of δB of the wave as

$$\delta B_\parallel = \delta B\, k_\perp\, C_s^2\, v_A^{-1}\, \omega_{pi}^{-1} \left(1 + \gamma_i k_\perp^2 r_{gi}^2\right)^{-1} \tag{36}$$

with plasma variables defined in section 3. For the solar wind parameters of Table 1 and for the Alfvén wave amplitude as a function of $k_\perp$ given by expressions (15a) and (15b), the magnitude of the Alfvén wave parallel magnetic field perturbation $\delta B_\parallel$ as given by expression (36) is plotted in green in Figure 12. Plotted for comparison is the perpendicular magnetic field perturbation $\delta B_\perp$ in blue. As can be seen, $\delta B_\parallel$ is usually small, but when $k_\perp \sim r_{gi}$, the parallel field $\delta B_\parallel$ of the wave becomes comparable to $\delta B_\perp$. Also plotted as the green points in Figure 12 is $\delta B_\parallel$ as a function of $k_\perp$ obtained from the linear Vlasov solutions.

[50] Comparing $B_{max} = B_o + \delta B_\parallel$ to $B_{min} = B_o - \delta B_\parallel$, a "mirror ratio" $R = B_{max}/B_{min}$ can be calculated, and from the mirror ratio the loss cone pitch angle $\alpha_{loss} = \text{asin}(R^{-1/2})$ (compare sections 2–8 of *Boyd and Sanderson* [1969]) can be calculated and the angular half-width $\Delta\alpha = 90° - \alpha_{loss}$ about 90° pitch angle of the population of mirroring particles can be calculated. That angular half-width $\Delta\alpha$ is plotted in dark red in Figure 12. Note that the angular width $\Delta\alpha$ of the population of mirroring particles is independent of kinetic energy and is the same for protons and electrons. For the solar wind parameters of Figure 12, $\Delta\alpha$ peaks at 7.6°, meaning electrons from pitch angles of 82.4° to 90° are trapped: For an isotropic population of electrons this represents 13% of all of the electrons being trapped.

[51] The nonlinear quenching of this transit time damping by an evolution of the velocity distribution function has not been considered here. Neither has the Coulomb scattering disruption of trapping between the Alfvén wave magnetic mirrors, which amounts to an angular scattering changing the electron pitch angle until it diffuses out of the mirroring region of pitch angle space.

6.4. Applicability of Linear Vlasov Calculations

[52] Owing to the nonzero parallel potential $\phi_\parallel$ of the Alfvén wave, electrons are trapped in the wave. Expression (31) (green curve in Figure 5) denotes the maximum electron velocity $\Delta v_\parallel = \Delta v_\parallel(\phi_\parallel)$ in the wave's reference frame of electrons trapped in the wave. In the rest frame of the plasma, electrons in the parallel velocity range from $v_\parallel = v_{ph} - \Delta v_\parallel$ to $v_\parallel = v_{ph} + \Delta v_\parallel$ are trapped in the wave. For $k_\perp r_{gi} = 0.1$ the range of the electron distribution function that is trapped is shaded in gray in Figure 13 (top).

[53] As shown in Figure 13, owing to the nonnegligible parallel potential of an Alfvén wave, the region of the electron distribution function containing electrons trapped in the wave can be substantial, with a velocity spread that is much larger than the phase velocity v_{ph} of the wave. And note that the parameters going into Figure 13 (which came from Figure 5) are for low-amplitude solar wind Alfvén waves: For higher-amplitude waves the trapping is more severe.

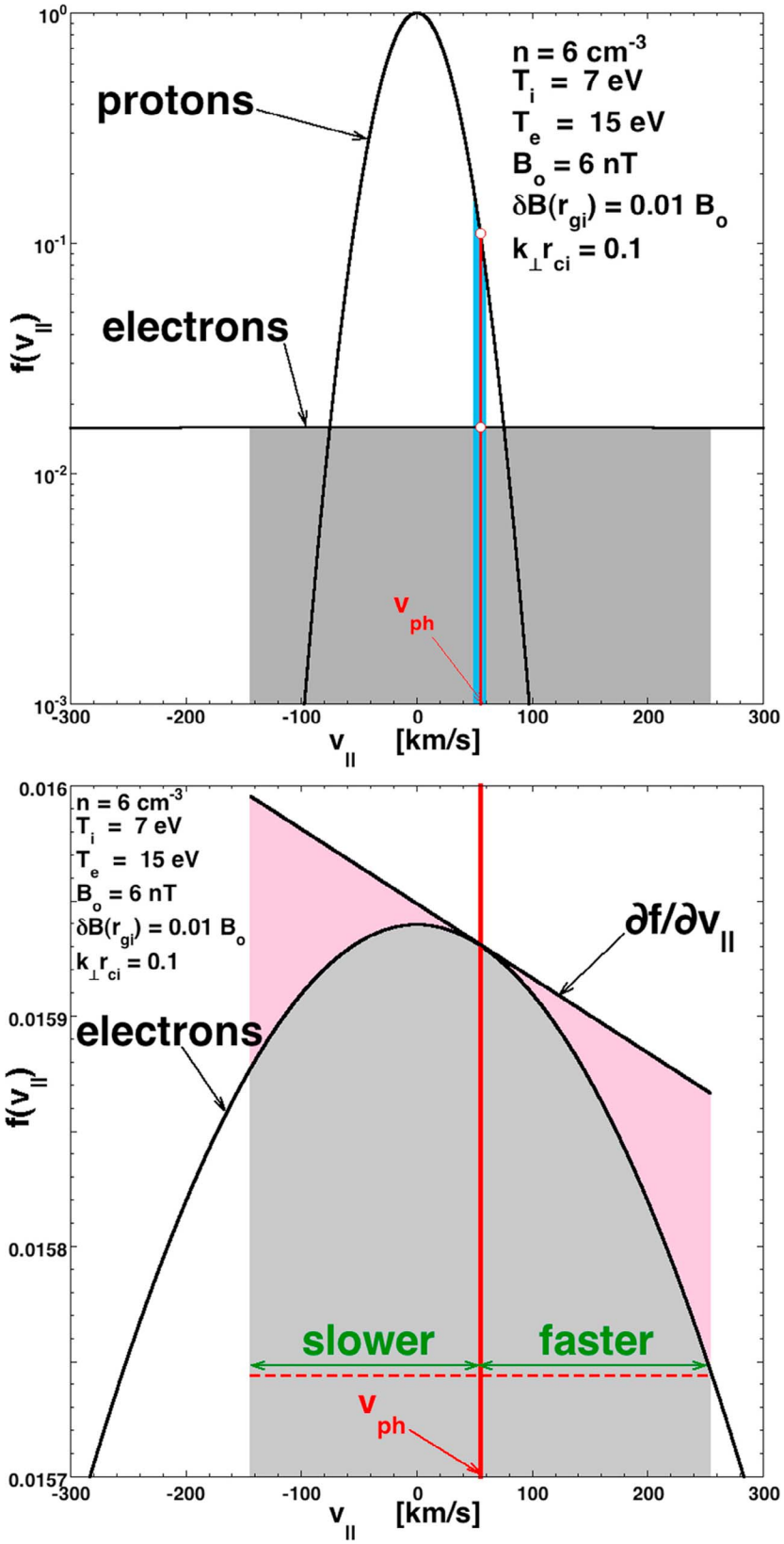

Figure 13. (top) A sketch of the electron and proton velocity distribution functions of the solar wind at 1 AU showing the widths of the electron and proton Landau resonances for $k_\perp r_{gi} = 0.1$. (bottom) The electron velocity distribution is redrawn for that resonance (note difference in vertical scale), and the $\partial f/\partial v_\parallel$ at $v_\parallel = v_{ph}$ tangent line is drawn in.

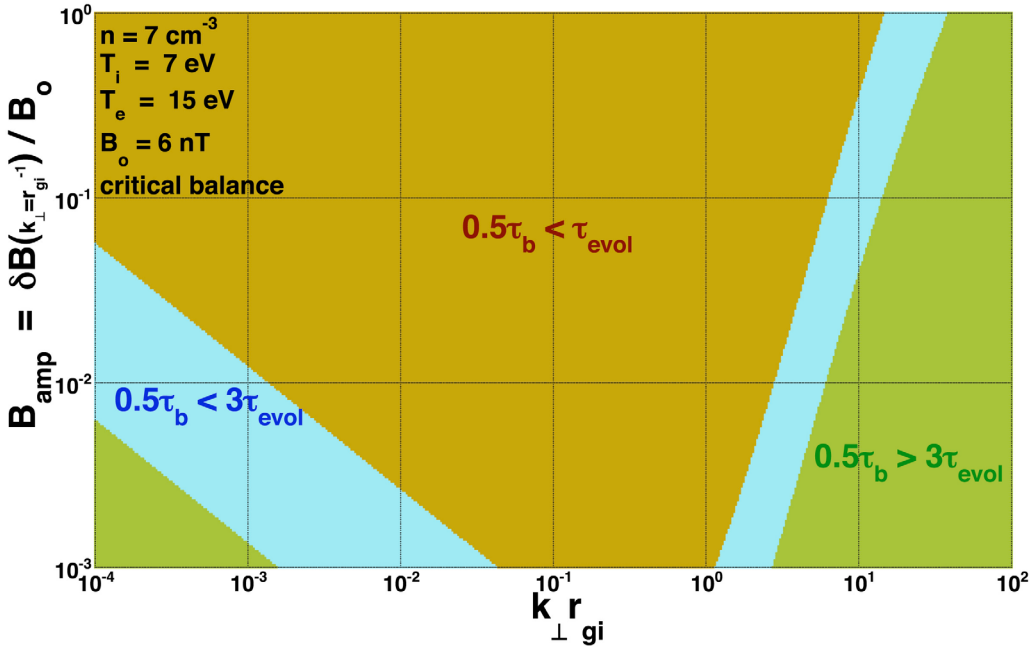

Figure 14. For Alfvén waves in the solar wind at 1 AU, the regions of $k_\perp$ where the trapped-electron bounce time is faster than the wave evolution time (brown), where the bounce time is slower than the wave evolution (green), and where the two times are comparable (blue) are plotted out as functions of the amplitude of the turbulence B_{amp}.

[54] In Figure 13 (bottom) the electron Maxwellian velocity distribution function is examined more closely. The Alfvén wave phase velocity v_{ph} is denoted by the red vertical line, and the trapped-electron range $v_{ph} - \Delta v_\parallel$ to $v_{ph} + \Delta v_\parallel$ is shaded in gray. The regions of resonant electrons "faster" than v_{ph} and "slower" than v_{ph} are indicated in green. The slope of the distribution function $\partial f/\partial v_\parallel$ at $v_\parallel = v_{ph}$ is indicated by the black line tangent to the distribution. By the trapezoidal rule the difference in the number of faster versus slower electrons is $\Delta v_\parallel\ \partial f/\partial v_\parallel$. When the trapping velocity $\Delta v_\parallel$ becomes large, $\partial f/\partial v_\parallel$ at $v_\parallel = v_{ph}$ is no longer an accurate indicator of the relative number of interacting electrons faster than the wave versus slower than the wave, unlike the case when the resonance width is small compared with the phase velocity [cf. *Nicholson*, 1983, section 6.7]. For $\Delta v_\parallel$ large, integration of the Maxwellian may be needed instead of a trapezoidal rule. (For the case of Figure 13, the faster-minus-slower error between integration and the trapezoidal rule is only 0.6%.) Hence, for $\Delta v_\parallel$ comparable to or larger than v_{ph}, the $\partial f/\partial v_\parallel$ coefficient of linear Landau damping may not be proportional to the actual damping decrement of the wave. Even if Coulomb collisions foil the trapping of individual electrons, the elements of the Maxwellian electron population that interact with the wave will still be over the broad range from $v_\parallel = v_{ph} - \Delta v_\parallel$ to $v_\parallel = v_{ph} + \Delta v_\parallel$, and this range will not be described by $\partial f/\partial v_\parallel$ at $v_\parallel = v_{ph}$.

[55] In the absence of collisions, one criterion for the validity of a linear Vlasov calculation of damping is that $\tau_L < \tau_b$, i.e., for the linear theory of damping to be valid the Landau-damping time scale τ_L must be shorter than the bounce time τ_b [*Dawson*, 1961; *O'Neil*, 1965; *Alexeff and Ishihara*, 1978] (see section 4.4.2 of *Davidson* [1972]). If the wave evolution process proceeds for a time longer than the bounce time, then electron orbits are no longer approximated by free-streaming (unaccelerated) orbits and the linear Vlasov analysis breaks down. As can be seen in Figure 7, bounce times in general are shorter than the linear-Landau-damping times, and so particle trapping invalidates the linear Vlasov estimate of the damping. Further, when the Alfvén wave spectrum of the solar wind is of larger amplitude than that considered here, the bounce times are more rapid and the case for linear Vlasov theory is worse.

[56] For a single wave, electrons are trapped in the wave's electrostatic potential. For a spectrum of waves, electrons can be detrapped if the coherence time or evolution time τ_{evol} of the fluctuations is fast compared with the bounce period τ_b of the trapped electrons [e.g., *Alexeff and Ishihara*, 1978; *Ryutov*, 1999]. The coherence time is the minimum of the wave-crossing time $\tau_{wave} = \lambda_\parallel/v_{ph}$ or the eddy turnover time $\tau_{eddy} = \lambda_\perp/\delta v_\perp$. Since we are considering fluctuations on the critical-balance curve, $\tau_{wave} = \tau_{eddy} = \tau_{evol}$. In Figure 7 the bounce period τ_b and the wave-crossing time τ_{wave} are plotted as the green and red curves, respectively. As can be seen, for $k_\perp r_{gi} < 1$ the two times are comparable. In this $k_\perp r_{gi} < 1$ regime it is expected that electrons will be trapped even in a spectrum of waves. Here, it may be improper to use linear Vlasov theory to calculate damping rates. As seen in Figure 7, for $k_\perp r_{gi} > 1$ the bounce time τ_b begins to be longer than the wave-crossing time τ_{wave}, so electrons might not be trapped. Here it is safer to use linear Vlasov theory.

[57] In Figure 14 the ratio of the bounce time τ_b to the evolution time $\tau_{evol} = \tau_{wave} = \tau_{eddy}$ is explored as a function of $k_\perp$ and of the amplitudes of the Alfvén waves. Regions where the electron crossing time $0.5\tau_b$ is shorter than the evolution time τ_{evol} are shaded in brown: Here electron trapping is important even in a spectrum of waves. Regions where the electron crossing time $0.5\tau_b$ is greater than three

evolution times $3\tau_{evol}$ are shaded in green in Figure 14: Here the Alfvénic fluctuations in a spectrum can evolve faster than the bouncing of trapped electrons. The regions shaded in blue with $\tau_{evol} < 0.5\tau_b < 3\tau_{evol}$ are transition regions where electron trapping will have an effect. In the brown and blue regions, linear Vlasov theory is not valid for calculating the electron-Landau-damping rates for Alfvénic fluctuations. In the green regions, which mostly pertain to $k_\perp > r_{gi}^{-1}$, linear Vlasov may be valid for the fluctuations in the spectrum. The horizontal line at $B_{amp} = 0.01$ in Figure 14 corresponds to Figure 7.

[58] Because the kinetic energies of protons that resonate with Alfvén waves in the solar wind are high (~20 eV), the width of the Landau resonance for protons should be narrow. And because the protons are massive, the proton bounce times should be long compared with wave evolution times. For these two reasons, linear Vlasov theory should be valid and accurate for calculating the proton-Landau-damping rates for Alfvén waves in the solar wind.

6.5. Potentials of Short-Wavelength Waves Disrupting Orbits in Long-Wavelength Waves

[59] Note in Figure 5 that even though the amplitudes of high-$k_\perp$ waves are much lower than the amplitudes of low-$k_\perp$ waves (see the blue δB curve), the parallel potentials within the high-$k_\perp$ waves greatly exceed the parallel potentials within the low-$k_\perp$ waves (see the red $\phi_\parallel$ curve). Hence, in a spectrum of fluctuations the large parallel potentials of the short-wavelength waves can interfere with particle motion in the long-wavelength waves. For the resonant electrons of a long-wavelength wave, instead of the "unperturbed" orbits (orbits in the absence of the wave) being unaccelerated free-streaming orbits or even electrons bouncing across the long-wavelength wave, the orbits will be electrons bouncing in short-wavelength waves between localized potential minima that propagate through the long-wavelength wave. Linear Vlasov theory is dubious here.

7. Discussion 2: Impact on Previous Work

[60] The scenario in which Landau damping at high-$k_\perp$ dissipates the $k_\perp$ cascade of energy in MHD turbulence [e.g., *Dobrowolny and Torricelli-Ciamponi*, 1985; *Leamon et al.*, 1999; *Gary and Borovsky*, 2004; *Howes et al.*, 2008] is unaffected, although the details of electron Landau damping at high-$k_\perp$ may be modified by the nonlinearities of the solar wind Alfvén waves. Ion Landau damping in high-β regions of the solar wind is particularly unmodified.

[61] The production of a shear viscosity for a large-scale collisionless plasma such as the solar wind by Alfvén wave Landau damping [cf. *Borovsky and Gary*, 2009] will still occur. For large-scale shears ($>10^5$ km) the previous calculations using linear Vlasov theory are accurate. However, for shear scales of less than ~10^5 km or less, detailed calculations for Landau damping in the presence of trapping and collisions need to be carried out to obtain accurate values of the viscosity. For a spectrum of fluctuations, electron trapping by short-wavelength fluctuations is an issue that needs to be considered in calculating the Landau-damping viscosity versus $k_\perp$.

[62] Coefficients for the Landau damping of Alfvén waves at high $k_\perp$ in the solar wind [e.g., *Gary and Borovsky*, 2008; *Podesta et al.*, 2010] need to be recalculated in light of the failure of linear Vlasov theory and the inaccuracy of $\partial f/\partial v_\parallel$ to represent faster versus slower resonant electron populations. At higher β, where ion Landau damping dominates over electron Landau damping, the previous calculations of the Landau-damping coefficients are probably accurate.

[63] **Acknowledgments.** The authors thank Joachim Birn, John Podesta, Ruth Skoug, and John Steinberg for useful conversations. This work was supported by the NASA Heliospheric SR&T Program, the NASA Heliospheric Guest-Investigator Program, and the NSF SHINE Program.

[64] Philippa Browning thanks the reviewers for their assistance in evaluating this paper.

References

Alexandrova, O., J. Saur, C. Lacombe, A. Mangeney, J. Mitchell, S. J. Schwartz, and P. Robert (2009), Universality of solar-wind turbulent spectrum from MHD to electron scales, *Phys. Rev. Lett.*, *103*, 165003, doi:10.1103/PhysRevLett.103.165003.

Alexeff, I., and O. Ishihara (1978), Landau damping for students, *IEEE Trans. Plasma Sci.*, *6*, 212, doi:10.1109/TPS.1978.4317111.

Alfvén, H., and C.-G. Falthammar (1963), *Cosmical Electrodynamics: Fundamental Principles*, *Int. Ser. Monogr. Phys.*, 228 pp., Oxford Univ. Press, London.

Asbridge, J. R., S. J. Bame, W. C. Feldman, and M. D. Montgomery (1976), Helium and hydrogen velocity differences in the solar wind, *J. Geophys. Res.*, *81*, 2719, doi:10.1029/JA081i016p02719.

Auerbach, S. P. (1977), Collisional damping of Langmuir waves in the collisionless limit, *Phys. Fluids*, *20*, 1836, doi:10.1063/1.861801.

Bilato, R., and M. Brambilla (2004), The role of collisions in the quasi-linear theory of radio-frequency heating and current drive in nearly collisionless plasmas, *Plasma Phys. Controlled Fusion*, *46*, 1455, doi:10.1088/0741-3335/46/9/008.

Bilato, R., and M. Brambilla (2008), On the nature of "collisionless" Landau damping, *Commun. Nonlinear Sci. Numer. Simul.*, *13*, 18, doi:10.1016/j.cnsns.2007.05.007.

Boldyrev, S. (2005), On the spectrum of magnetohydrodynamic turbulence, *Astrophys. J.*, *626*, L37, doi:10.1086/431649.

Borovsky, J. E. (1993), Auroral arc thicknesses as predicted by various theories, *J. Geophys. Res.*, *98*, 6101, doi:10.1029/92JA02242.

Borovsky, J. E. (2008), Flux tube texture of the solar wind: Strands of the magnetic carpet at 1 AU?, *J. Geophys. Res.*, *113*, A08110, doi:10.1029/2007JA012684.

Borovsky, J. E. (2010), On the variations of the solar wind magnetic field about the Parker spiral direction, *J. Geophys. Res.*, *115*, A09101, doi:10.1029/2009JA015040.

Borovsky, J. E., and M. H. Denton (2010), Solar-wind turbulence and shear: A superposed-epoch analysis of corotating interaction regions at 1 AU, *J. Geophys. Res.*, *115*, A10101, doi:10.1029/2009JA014966.

Borovsky, J. E., and S. P. Gary (2009), On viscosity and the Reynolds number of MHD turbulence in collisionless plasmas: Coulomb collisions, Landau damping, and Bohm diffusion, *Phys. Plasmas*, *16*, 082307, doi:10.1063/1.3155134.

Bostrom, R. (1973), Electrodynamics of the ionosphere, in *Cosmical Geophysics*, edited by A. Egeland, O. Holter, and A. Omholt, 181 pp., Universitetsforlaget, Oslo.

Boyd, T. J. M., and J. J. Sanderson (1969), *Plasma Dynamics*, 348 pp., Nelson, London.

Braginskii, S. I. (1965), Transport processes in a plasma, in *Reviews of Plasma Physics*, vol. 1, edited by M. A. Leontovich, 205 pp., Consult. Bur., New York.

Bruno, R., V. Carbone, P. Veltri, E. Pietropaolo, and B. Bavassano (2001), Identifying intermittency events in the solar wind, *Planet. Space Sci.*, *49*, 1201, doi:10.1016/S0032-0633(01)00061-7.

Burgers, J. M. (1963), Application of the two-particle distribution functions to estimate the collisional damping of plasma oscillations, *Phys. Fluids*, *6*, 889, doi:10.1063/1.1706843.

Burlaga, L. F. (1968), Micro-scale structures in the interplanetary medium, *Sol. Phys.*, *4*, 67, doi:10.1007/BF00146999.

Burlaga, L. F. (1969), Directional discontinuities in the interplanetary magnetic field, *Sol. Phys.*, *7*, 54, doi:10.1007/BF00148406.

Burlaga, L. F. (1971), Nature and origin of directional discontinuities in the solar wind, *J. Geophys. Res.*, *76*, 4360, doi:10.1029/JA076i019p04360.

Comisar, G. G. (1963), Collisional damping of plasma oscillations, *Phys. Fluids*, *6*, 76, doi:10.1063/1.1724511.
Davidson, R. C. (1972), *Methods in Nonlinear Plasma Physics*, Academic, New York.
Dawson, J. (1961), On Landau damping, *Phys. Fluids*, *4*, 869, doi:10.1063/1.1706419.
Denavit, J., B. W. Doyle, and R. H. Hirsch (1968), Nonlinear and collisional effects on Landau damping, *Phys. Fluids*, *11*, 2241, doi:10.1063/1.1691808.
Denton, M. H., and J. E. Borovsky (2008), Superposed epoch analysis of high-speed-stream effects at geosynchronous orbit: Hot plasma, cold plasma, and the solar wind, *J. Geophys. Res.*, *113*, A07216, doi:10.1029/2007JA012998.
Dobrowolny, M., and G. Torricelli-Ciamponi (1985), Alfvén wave dissipation in the solar wind, *Astron. Astrophys.*, *142*, 404.
Fejer, J. A., and J. R. Kan (1969), A guiding centre Vlasov equation and its application to Alfvén waves, *J. Plasma Phys.*, *3*, 331, doi:10.1017/S0022377800004438.
Feldman, W. C., J. R. Asbridge, S. J. Bame, and M. D. Montgomery (1973), Double ion streams in the solar wind, *J. Geophys. Res.*, *78*, 2017, doi:10.1029/JA078i013p02017.
Feldman, W. C., J. R. Asbridge, S. J. Bame, M. D. Montgomery, and S. P. Gary (1975), Solar wind electrons, *J. Geophys. Res.*, *80*, 4181, doi:10.1029/JA080i031p04181.
Gary, S. P. (1967), Third-order oscillations in a Maxwellian plasma, *Phys. Fluids*, *10*, 570, doi:10.1063/1.1762150.
Gary, S. P., and J. E. Borovsky (2004), Alfvén-cyclotron fluctuations: Linear Vlasov theory, *J. Geophys. Res.*, *109*, A06105, doi:10.1029/2004JA010399.
Gary, S. P., and J. E. Borovsky (2008), Damping of long-wavelength kinetic Alfvén fluctuations: Linear theory, *J. Geophys. Res.*, *113*, A12104, doi:10.1029/2008JA013565.
Gary, S. P., and K. Nishimura (2004), Kinetic Alfvén waves: Linear theory and particle-in-cell simulation, *J. Geophys. Res.*, *109*, A02109, doi:10.1029/2003JA010239.
Goertz, C. K. (1984), Kinetic Alfvén waves on auroral field lines, *Planet. Space Sci.*, *32*, 1387, doi:10.1016/0032-0633(84)90081-3.
Goertz, C. K., and R. W. Boswell (1979), Magnetosphere-ionosphere coupling, *J. Geophys. Res.*, *84*, 7239, doi:10.1029/JA084iA12p07239.
Goldreich, P., and S. Sridhar (1997), Magnetohydrodynamic turbulence revisited, *Astrophys. J.*, *485*, 680, doi:10.1086/304442.
Hasegawa, A. (1977), Kinetic properties of Alfvén waves, *Proc. Indiana Acad. Sci.*, *86A*, 151.
Hasegawa, A., and L. Chen (1976), Parametric decay of "kinetic Alfvén wave" and its application to plasma heating, *Phys. Rev. Lett.*, *36*, 1362, doi:10.1103/PhysRevLett.36.1362.
Hedrick, C. L., J.-N. Lebouef, and D. A. Spong (1995), Shear Alfvén waves with Landau and collisional effects, *Phys. Plasmas*, *2*, 2033, doi:10.1063/1.871291.
Hollweg, J. V. (1999), Kinetic Alfvén wave revisited, *J. Geophys. Res.*, *104*, 14,811, doi:10.1029/1998JA900132.
Horbury, T. S., M. Forman, and S. Oughton (2008), Anisotropic scaling of magnetohydrodynamic turbulence, *Phys. Rev. Lett.*, *101*, 175005, doi:10.1103/PhysRevLett.101.175005.
Howes, G. G., S. C. Cowley, W. Dorland, G. W. Hammett, E. Quataert, and A. A. Schekochihin (2008), A model of turbulence in magnetized plasmas: Implications for the dissipation range in the solar wind, *J. Geophys. Res.*, *113*, A05103, doi:10.1029/2007JA012665.
Isensee, U., and H. Maassberg (1981), Particle-in-cell simulation of the plasma environment of a spacecraft in the solar wind, *Adv. Space Res.*, *1*, 413, doi:10.1016/0273-1177(81)90315-X.
Johnston, G. L. (1971), Dominant effects of Coulomb collisions on maintenance of Landau damping, *Phys. Fluids*, *14*, 2719, doi:10.1063/1.1693397.
Kaganovich, I. D. (1999), Effects of collisions and particle trapping on collisionless heating, *Phys. Rev. Lett.*, *82*, 327, doi:10.1103/PhysRevLett.82.327.
Katz, I., M. Mandell, B. Gardner, and R. Maurer (2001), MESSENGER spacecraft charging analysis, *ESA SP-476*, p. 101, Eur. Space Agency, Noordwijk, Netherlands.
Knorr, G. (1963), Zur Losung der Nicth-linearen Vlasov-Gleichung, *Z. Naturforsch.*, *18a*, 1304.
Krall, N. A., and A. W. Trivelpiece (1973), *Principles of Plasma Physics*, McGraw-Hill, New York.
Lacombe, C., C. Salem, A. Mangeney, D. Hubert, C. Perche, J.-L. Bougeret, P. J. Kellogg, and J.-M. Bosqued (2002), Evidence for the interplanetary electric potential? WIND observations of electrostatic fluctuations, *Ann. Geophys.*, *20*, 609, doi:10.5194/angeo-20-609-2002.
Leamon, R. J., C. W. Smith, N. F. Ness, W. H. Matthaeus, and H. K. Wong (1998), Observational constraints on the dynamics of the interplanetary magnetic field dissipation range, *J. Geophys. Res.*, *103*, 4775, doi:10.1029/97JA03394.
Leamon, R. J., C. W. Smith, N. F. Ness, and H. K. Wong (1999), Dissipation range dynamics: Kinetic Alfvén waves and the importance of β_e, *J. Geophys. Res.*, *104*, 22,331, doi:10.1029/1999JA900158.
Lemaire, J., and M. Scherer (1971), Kinetic models of the solar wind, *J. Geophys. Res.*, *76*, 7479, doi:10.1029/JA076i031p07479.
Lessard, M. R., and D. J. Knudsen (2001), Ionospheric reflection of small-scale Alfvén waves, *Geophys. Res. Lett.*, *28*, 3573, doi:10.1029/2000GL012529.
Lysak, R. L., and W. Lotko (1996), On the kinetic dispersion relation for shear Alfvén waves, *J. Geophys. Res.*, *101*, 5085, doi:10.1029/95JA03712.
Mangeney, A., C. Salem, C. Lacombe, J.-L. Bougeret, C. Perche, R. Manning, P. J. Kellogg, K. Goetz, S. J. Monson, and J.-M. Bosqued (1999), WIND observations of coherent electrostatic waves in the solar wind, *Ann. Geophys.*, *17*, 307, doi:10.1007/s00585-999-0307-y.
Marsch, E. (2006), Kinetic physics of the solar corona and solar wind, *Living Rev. Sol. Phys.*, *3*, 1.
Marsch, E., K.-H. Mühlhäuser, H. Rosenbauer, R. Schwenn, and F. M. Neubauer (1982a), Solar wind helium ions: Observations of the Helios solar probes between 0.3 and 1 AU, *J. Geophys. Res.*, *87*, 35, doi:10.1029/JA087iA01p00035.
Marsch, E., K.-H. Mühlhäuser, R. Schwenn, H. Rosenbauer, W. Pilipp, and F. M. Neubauer (1982b), Solar wind protons: Three-dimensional velocity distributions and derived plasma parameters measured between 0.3 and 1 AU, *J. Geophys. Res.*, *87*, 52, doi:10.1029/JA087iA01p00052.
Medvedev, M. V. (1999), Collisionless dissipative nonlinear Alfvén waves: Nonlinear steepening, compressible turbulence, and particle trapping, *Phys. Plasmas*, *6*, 2191, doi:10.1063/1.873471.
Medvedev, M. V., P. H. Diamond, M. N. Rosenbluth, and V. I. Shevchenko (1998), Asymptotic theory of nonlinear Landau damping and particle trapping in waves of finite amplitude, *Phys. Rev. Lett.*, *81*, 5824, doi:10.1103/PhysRevLett.81.5824.
Mitchner, M., and C. H. Kruger (1973), *Partially Ionized Gases*, section 8.7, John Wiley, New York.
Narita, Y., K.-H. Glassmeier, F. Sahraoui, and M. L. Goldstein (2010), Wave-vector dependence of magnetic-turbulence spectra in the solar wind, *Phys. Rev. Lett.*, *104*, 171101, doi:10.1103/PhysRevLett.104.171101.
Neufeld, J., and R. H. Ritchie (1955), Passage of charged particles through plasma, *Phys. Rev.*, *98*, 1632, doi:10.1103/PhysRev.98.1632.
Neugebauer, M. M., and W. C. Feldman (1979), Relation between superheating and superacceleration of helium in the solar wind, *Sol. Phys.*, *63*, 201, doi:10.1007/BF00155710.
Nicholson, D. R. (1983), *Introduction to Plasma Physics*, John Wiley, New York.
O'Neil, T. (1965), Collisionless damping of nonlinear plasma oscillations, *Phys. Fluids*, *8*, 2255, doi:10.1063/1.1761193.
Parashar, T. N., M. A. Shay, P. A. Cassak, and W. H. Matthaeus (2009), Kinetic dissipation and anisotropic heating in a turbulent collisionless plasma, *Phys. Plasmas*, *16*, 032310, doi:10.1063/1.3094062.
Pierrard, V., K. Issautier, N. Meyer-Vernet, and J. Lemaire (2001), Collisionless model of the solar wind in a spiral magnetic field, *Geophys. Res. Lett.*, *28*, 223, doi:10.1029/2000GL011888.
Podesta, J. J. (2009), Dependence of solar-wind power spectra on the direction of the local mean magnetic field, *Astrophys. J.*, *698*, 986, doi:10.1088/0004-637X/698/2/986.
Podesta, J. J. (2011), On the energy cascade rate of solar wind turbulence in high cross helicity flows, *J. Geophys. Res.*, *116*, A05101, doi:10.1029/2010JA016306.
Podesta, J. J., and J. E. Borovsky (2010), Scale invariance of normalized cross-helicity throughout the inertial range of solar wind turbulence, *Phys. Plasmas*, *17*, 112905, doi:10.1063/1.3505092.
Podesta, J. J., D. A. Roberts, and M. L. Goldstein (2007), Spectral exponents of kinetic and magnetic energy spectra in solar wind turbulence, *Astrophys. J.*, *664*, 543, doi:10.1086/519211.
Podesta, J. J., J. E. Borovsky, and S. P. Gary (2010), A kinetic Alfvén wave cascade subject to collisionless damping cannot reach electron scales in the solar wind at 1 AU, *Astrophys. J.*, *712*, 685, doi:10.1088/0004-637X/712/1/685.
Potapenko, I. F., C. A. de Azevedo, and P. H. Sakanaka (2000), Electron heating and acceleration by Alfvén waves with varying phase velocity, *Phys. Scr.*, *62*, 486, doi:10.1238/Physica.Regular.062a00486.
Riazantseva, M. O., G. N. Zastenker, and J. D. Richardson (2005), The characteristics of sharp (small-scale) boundaries of solar wind plasma and magnetic field structures, *Adv. Space Res.*, *35*, 2147, doi:10.1016/j.asr.2004.12.011.
Roberts, D. A. (2010), Evolution of the spectrum of solar wind magnetic and velocity fluctuations from 0.3 to 5 AU, *J. Geophys. Res.*, *115*, A12101, doi:10.1029/2009JA015120.

Ryutov, D. D. (1999), Landau damping: Half a century with the great discovery, *Plasma Phys. Controlled Fusion*, *41*, A1, doi:10.1088/0741-3335/41/3A/001.

Sahraoui, F., M. L. Goldstein, P. Robert, and Y. V. Khotyaintsev (2009), Evidence of a cascade and dissipation of solar-wind turbulence at the electron gyroscale, *Phys. Rev. Lett.*, *102*, 231,102, doi:10.1103/PhysRevLett.102.231102.

Sahraoui, F., M. L. Goldstein, G. Belmont, P. Canu, and L. Rezeau (2010), Three dimensional anisotropic k spectra of turbulence at subproton scales in the solar wind, *Phys. Rev. Lett.*, *105*, 131,101, doi:10.1103/PhysRevLett.105.131101.

Salem, C., J.-M. Bosqued, D. E. Larson, A. Mangeney, M. Maksimovic, C. Perche, R. P. Lin, and J.-L. Bougeret (2001), Determination of accurate solar wind electron parameters using particle detectors and radio wave receivers, *J. Geophys. Res.*, *106*, 21,701, doi:10.1029/2001JA900031.

Salem, C., C. Lacombe, A. Mangeney, P. J. Kellogg, and J.-L. Bougeret (2003), Weak double layers in the solar wind and their relation to the interplanetary electric field, *AIP Conf. Proc.*, *679*, 513.

Scime, E. E., J. L. Phillips, and S. J. Bame (1994), Effects of spacecraft potential on three-dimensional electron measurements in the solar wind, *J. Geophys. Res.*, *99*, 14,769, doi:10.1029/94JA00489.

Scott, W. T. (1963), The theory of small-angle multiple scattering of fast charged particles, *Rev. Mod. Phys.*, *35*, 231, doi:10.1103/RevModPhys.35.231.

Shkarofsky, I. P., T. W. Johnston, and M. P. Bachynski (1966), *The Particle Kinetics of Plasmas*, Addison-Wesley, Reading, Mass.

Skoug, R. M., W. C. Feldman, J. T. Gosling, D. J. McComas, and C. W. Smith (2000), Solar wind electron characteristics inside and outside coronal mass ejections, *J. Geophys. Res.*, *105*, 23,069, doi:10.1029/2000JA000017.

Smith, C. W., K. Hamilton, B. J. Vasquez, and R. J. Leamon (2006), Dependence of the dissipation range spectrum of interplanetary magnetic fluctuations on the rate of energy cascade, *Astrophys. J.*, *645*, L85, doi:10.1086/506151.

Sorriso-Valvo, L., V. Carbone, R. Bruno, and P. Veltri (2006), Persistence of small-scale anisotropy of magnetic turbulence as observed in the solar wind, *Europhys. Lett.*, *75*, 832, doi:10.1209/epl/i2006-10172-y.

Stéfant, R. J. (1970), Alfvén wave damping from finite gyroradius coupling to the ion acoustic mode, *Phys. Fluids*, *13*, 440, doi:10.1063/1.1692938.

Stepanov, K. N. (1958), Kinetic theory of magnetohydrodynamic waves, *Sov. Phys. JETP, Engl. Transl.*, *34*, 892.

Thompson, B. J., and R. L. Lysak (1996), Electron acceleration by inertial Alfvén waves, *J. Geophys. Res.*, *101*, 5359, doi:10.1029/95JA03622.

Wicks, R. T., T. S. Horbury, C. H. K. Chen, and A. A. Schekochihin (2010), Power and spectral index anisotropy of the entire inertial range of turbulence in the fast solar wind, *Mon. Not. R. Astron. Soc.*, *407*, L31, doi:10.1111/j.1745-3933.2010.00898.x.

Zakharov, V. E., and V. I. Karpman (1963), On the nonlinear theory of the damping of plasma waves, *Sov. Phys. JETP, Engl. Transl.*, *16*, 351.

J. E. Borovsky and S. P. Gary, Space Science and Applications, Los Alamos National Laboratory, Mail Stop D466, Los Alamos, NM 87545, USA. (jborovsky@lanl.gov)